When Less is MORE: Counterintuitive Stoichiometries and Cellular Abundances are Essential for ABC transporters' function

Short title

Functional-Proteomics of ABC Importers

Hiba Qasem Abdullah[1], Nurit Livnat Levanon[1*], Michal Perach[1], Moti Grupper [2], Tamar Ziv[3], and Oded Lewinson[1]*

[1] Department of Molecular Microbiology, Bruce and Ruth Rappaport Faculty of Medicine, Technion-Israel Institute of Technology, Haifa, Israel.

[2] Infectious Disease Unit, Rambam Health Care Campus, Haifa, Israel.

3 Smoler Proteomics Center, Technion-Israel Institute of Technology, Haifa, Israel.

[*]Equal contribution

For correspondence: lewinson@technion.ac.il

Abstract

Prokaryotes acquire essential nutrients primarily through ABC importers, consisting of an ATPase, a permease, and a substrate-binding protein. These importers are highly underrepresented in proteomic databases, limiting our knowledge about their cellular copy numbers, component stoichiometry, and the mechanistic implications of these parameters. We developed a tailored proteomic approach to compile the most comprehensive dataset to date of the *E. coli* 'ABC importome'. Functional assays and analysis of deletion strains revealed mechanistic features linking molecular mechanisms to cellular abundances, co-localization, and component stoichiometries. We observed 4-5 orders of magnitude variation in import system abundances, with copy numbers tuned to nutrient hierarchies essential for growth. Abundances of substrate-binding proteins are unrelated to their substrate binding affinities but are tightly, yet inversely, correlated with their interaction affinity with permeases. Counterintuitive component stoichiometries are crucial for function, offering insights into the design principles of multi-component protein systems, potentially extending beyond ABC importers.

Teaser

Bacteria's nutrient absorption secrets unveiled: deciphering the complexity of ABC impoters required for optimal growth.

Introduction

ATP-binding cassette (ABC) transporters comprise one of the largest and oldest protein families of any proteome, with ~120 members in higher plants, 49 in human, and ~80 in prokaryotes. They harness the energy of ATP hydrolysis to move molecules across cell membranes (*1*). In humans, ABC transporters protect cells from toxic materials and deliver biomolecules to designated compartments. They are directly linked to human diseases and to tumor chemotherapy resistance (*2*, *3*). In prokaryotes, the high-affinity acquisition of nutrients is mediated by ABC transporters that function as importers (hereafter ABC importers). Each ABC importer is highly specific to a single nutrient or a group of highly similar nutrients. Under conditions of nutrient limitation, such as those encountered during host infection, their role is underscored. It is therefore not surprising that a large number of bacterial ABC importers have been identified as key virulence determinants (*4*, *5*).

The functional unit of an ABC transporter minimally consists of four domains: two transmembrane domains (TMDs) that form the translocation pathway and two cytoplasmic nucleotide-binding domains (NBDs) that provide energy via ATP hydrolysis. ABC importers additionally require a substrate binding protein (SBP) which binds the substrate and delivers it to its cognate transporter (*6*).

Knowledge of absolute protein levels (*i.e.*, copy number per cell and protein cellular concentrations) is essential for kinetic modeling of biological processes, for comparing concentrations of different proteins within or across samples or species and for quantifying protein-level adaptations to changes in internal or external conditions (*7–11*). As ABC importers provide the main route for prokaryotic nutrient import any quantitative study of cellular metabolite influx or metabolism/anabolism balance must consider their copy number. For multi-component systems such as ABC importers, other parameters that need to be considered are component stoichiometry and component localization/co-localization (*12–14*).

Bacterial ABC importers are heavily underrepresented in current proteomic datasets (*11*, *15–18*). In addition, in contrast to human ABC transporters (*19*, *20*) and other protein families (*21–25*), prokaryotic ABC importers have not been specifically targeted by proteomic studies. Therefore, we still lack a rigorous understanding of their copy number and stoichiometries and of the mechanistic implications of these parameters.

Herein, we developed a tailored protocol for the label-free tandem mass spectrometry (LC-MS^2) quantification of ABC importers and compile a comprehensive dataset detailing their cellular copy numbers and component stoichiometries. Based on this proteomic data, we performed functional assays and identified unexpected mechanistic features of ABC importers, linking molecular mechanisms and physiological roles to cellular copy numbers and component stoichiometries.

Results and discussion

Compilation of the ABC importome dataset

A search of the EcoCyc database (*26*) identified 47 ABC import systems in the genome of *E. coli* K12 strain BW25113. These systems, hereafter referred to as the ABC importome (Table S1), are encoded by 175 genes, encoding 47 substrate-binding proteins (SBPs), 54 nucleotide-binding domains (NBDs), and 74 transmembrane domains (TMDs). This composition reflects that all SBPs function as monomers. Unlike the SBPs, which function as monomers, the NBDs and TMDs function as dimers. Among the NBDs, 7 systems are heterodimeric, while 40 are homodimeric. The TMDs exhibit a greater tendency for heterodimerization, with 27 systems being heterodimeric and 20 homodimeric.

The 175 proteins that comprise the ABC importome remain underrepresented in the 18 available *E. coli* proteomic datasets (https://pax-db.org/). Moreover, reported abundances of many components can vary by up to 500-fold across different datasets. These variations may, in part, arise from the use of different growth media, as reported by the Heinemann group (*11*). However, even when identical media are used, substantial discrepancies between studies persist (*16*, *27*, *28*), likely due to technical differences, including sample preparation protocols, proteolytic cleavage efficiency, detergent content, and detection sensitivity.

These inconsistencies complicate the integration of such disparate data. Therefore, our goal was to compile a unified dataset that offers a comprehensive overview of the relative abundances of the components of the ABC importome.

We used the *E. coli* K12 strain BW25113, the progenitor strain of the Keio clone collection (*29*), a strain utilized in multiple proteomic investigations (*11*, *30–32*). Cultures were cultivated in M9-glucose medium to mid-exponential phase, harvested by centrifugation, and stored in -80°C until use.

Initially, LC-MS^2 analysis samples were prepared following a protocol based on SDS/urea extraction and denaturation, followed by tryptic digestion. Briefly, the extracts were dissolved in buffer containing 10 mM DTT and 5% SDS, sonicated and boiled prior to acetone precipitation. Subsequently, the pellets were dissolved in Urea/ammonium bicarbonate, reduced with DTT, and modified with iodoacetamide. Digestion was carried out overnight in the presence of Urea/ammonium bicarbonate using trypsin (see methods for full details).

As observed by others (*11*, *33*), using this standard urea-SDS-trypsin sample preparation protocol we failed to identify many of the transmembrane domains (Table S2). Missing transmembrane domains (TMDs) of special interest included those of the import systems for maltose (MalFGK), histidine (HisPQM), vitamin B_{12} (BtuCD), zinc (ZnuBC), and molybdate (MolBC).

Since the standard urea-SDS-trypsin sample preparation protocol did not lead to satisfactory coverage, we tested alternative protocols. We modified three key sample preparation parameters: 1) protease, 2) detergent, and 3) membrane washing agents. Beyond trypsin, we explored digestion with chymotrypsin, pepsin, LysC, WalP, and Proanalase, all of which have been reported as promising

alternatives for the proteomic analysis of membrane proteins (*34*, *35*). In parallel, and in combination, we tested detergents other than SDS, such as n-Dodecyl-β-Maltoside (DDM), n-Decyl-β-Maltoside (DM), and their mixtures. In our experience, SDS often causes aggregation and sedimentation of ABC transporters, a problem rarely encountered with maltoside-based detergents.

Additionally, we prepared membrane fractions from the same cell pellets and, and for further enrichment, tested washing the membranes with high salt, EDTA, or sodium bicarbonate—agents known to remove loosely attached proteins and enhance the proteomic coverage of membrane proteins. Table S2 lists the components of the ABC importome identified using several of these alternative protocols.

The most substantial improvement came from the preparation of membrane fractions, which enabled the identification of 14 proteins previously masked by the complexity of the whole-cell proteome. Other notable improvements were achieved by washing membranes with 100 mM sodium bicarbonate or using chymotrypsin instead of trypsin, which led to the identification of 7 and 9 additional components, respectively.

Unfortunately, no single sample preparation protocol achieved the desired target proteomic coverage of over 70%. As an alternative, we chose to merge datasets obtained from different protocols. To do this, we first identified datasets with high correlation, indicating their suitability for merging.

As shown, we observed excellent correlations between technical and biological replicates (Figure S1A and S1B, respectively). Furthermore, a strong correlation was evident between the intensities of membrane proteins measured in whole cells and those in membrane fractions prepared from the same cells (Figure S1C), as well as between membrane protein intensities measured in membrane fractions and those measured in the same membranes washed in 100 mM sodium bicarbonate (Figure S1D). In contrast, we observed low to moderate correlations between samples digested with trypsin and those digested with chymotrypsin, LysC, pepsin, or Proanalse (Figure S2A-D). Similarly, we noted low correlations between samples extracted with SDS and those extracted with n-Dodecyl-β-D-maltoside (DDM), n-Decyl-β-Maltoside (DM), or a mixture of DM and DDM (Figure S3A-C). Based on these findings, we concluded that MS spectra obtained from biological replicates, membrane fractions, and membrane fractions washed with sodium bicarbonate can be integrated to form a unified dataset. In contrast, spectra acquired using alternative proteases or detergents could not be reliably combined.

Subsequently, we determined the fractional mass for each protein by utilizing its relative Intensity-Based Absolute Quantification value (*riBAQ*,(*36*, *37*)) and the known total protein content in the sample. These fractional masses were then converted to copy numbers employing the molecular weights of the proteins and Avogadro's number. The ABC importome components were integrated into a consolidated dataset using the slopes of the correlation curves (Figure S1A-D), and cellular copy numbers were derived by dividing the total copy number of each protein by the number of cells as determined through colony

counting. The complete mathematical expressions for these conversions are provided in the methods section.

Next, we wished to authenticate the cellular copy numbers we determined. First, we compared our estimated cellular copy numbers with those from four other proteomic studies, which used label-free LC-MS^2 quantification (*38*, *39*), labeled peptides as internal standers (*11*), or Stable Isotope Labeling by Amino Acids in Cell Culture (SILAC) quantification (*40*). For this comparison, we focused on substrate binding proteins (SBPs) since, unlike the transmembrane domains (TMDs) and nucleotide-binding domains (NBDs), identifying SBPs did not require additional sample processing steps (*e.g.*, preparation of membrane fractions and membrane washing with sodium carbonate), which were only applied in our study. Figure S4 shows that our cellular copy numbers correlate reasonably with these studies (coefficient of determination (R^2) 0.61-0.81). However, these correlations should be interpreted cautiously, as they are skewed by outlier data points. For instance, in Figure S4A, removing the two highest-value data points reduces the R^2 from 0.81 to 0.58. Nevertheless, our study demonstrates stronger correlations with each of the four additional studies than they do with one another (compare Figures S4 and S5). Collectively, these results suggest that the quality of our comprehensive dataset is on par with what has been reported to date.

To validate the reported cellular copy numbers in a more quantitative way we used purified proteins as standards. We chose eight components of the ABC importome that we have purified in the past. Using our established protocols (*41–43*), we purified three SBPs (MetQ, FliY, BtuF), three NBDs (MetN, YecS, BtuD), and two TMDs (MetI, YecC), representing proteins of low, medium, and high abundance. Each protein was digested separately with trypsin, and a mixture containing equal molar amounts of the digested proteins was prepared and desalted. A sample from this mixture was then analyzed by LC-MS^2, and the ratio between the measured intensity of each purified protein and its molar amount was used to convert the intensity measured in whole-cell samples into molar quantities. These molar amounts were then compared to the molar amounts calculated using iBAQ quantification. For complete details of how this comparison was conducted see the methods section and Table S3.

As shown (Figure 1), we observed excellent agreement between the iBAQ quantification from whole-cell lysates and the quantification using purified protein standards.

Collectively, these results suggest that the data provide a reliable estimate of the cellular copy numbers for the components of the ABC importome. Our final dataset (Table S4) includes 42 SBPs, 38 TMDs, and 33 NBDs, covers approximately 65% of the ABC importome and represents the most comprehensive coverage to date.

Abundances of the components of the ABC importome

Figure 2A shows the cellular copy numbers of the substrate binding proteins (SBPs) we identified, and the first striking feature that we noticed was the large variation in their abundances, spanning over more than four orders of magnitude (from nM to low mM concentrations). The most abundant SBPs, with approximately 20,000 copies per cell (resulting in a periplasmic concentration of ~0.1 mM), were LivJ (Leu/Ile/Val SBP) and MetQ (L-Met SBP). In contrast, the least abundant SBPs, with an average of 1-3 molecules per cell (equating to a periplasmic concentration of approximately 2-6 nM), were BtuF and FhuD (vitamin B12 and ferric hydroxamate SBPs, respectively). To ensure that the estimated cellular copy numbers were not specific to quantification of trypsin-derived peptides, we repeated the experiments and analysis using chymotrypsin. Reassuringly, as shown in Figure S6A, similar abundances were observed with both proteases.

We hypothesized that this substantial variability might be related to the substrate binding affinity, where high abundances could potentially compensate for low substrate-binding affinities. However, as illustrated in Figure 2B, we did not observe such a correlation. For instance, the highly abundant SBP, MetQ, exhibits a very high affinity for methionine (~0.2 nM, (*44*)), whereas FliY, which is approximately four-fold less abundant, binds cysteine/cystine with a 50,000-fold lower affinity of ~ 10 μM (*43*).

An alternative driving force that may influence SBP abundance is the affinity of their interaction with their cognate transporters. SBPs that interact with low affinity may be present at higher concentrations, while those with high affinity may be present at lower concentrations. Only seven values of SBP-transporter interaction affinity have been reported to date (*41*, *45–49*). However, despite this paucity of information we observed a clear correlation between the SBP-transporter interaction affinities and copy number, with high interaction affinities strongly correlating with SBPs of low abundance and low interaction affinities strongly correlating with high SBPs abundances (Figure 2C). A similar correlation between high interaction affinity and low SBP abundance was observed when chymotrypsin was used, suggesting that this is a general phenomenon and not specific to the choice of protease (Figure S6B).

It is difficult to resolve the chicken and the egg in this phenomenon: do low SBP abundances dictate high interaction affinities with the transporter or did high interaction affinities provide a selective pressure for reduced abundances. Whatever is the cause-effect relation, these two variables seem to be tightly linked.

In terms of abundance, the SBPs segregate into four distinct groups (Figure 2A, Figure S6A): The most abundant SBPs are those binding peptides and amino acids. This observation aligns with the high cellular demand for amino acids (*50*) and with findings indicating that protein synthesis is the energetically most demanding cellular process (*51*). The second most abundant group consists of SBPs binding sugars, which are also required in substantial amounts. As glucose served as the carbon source for growing the cultures, the lower abundance of sugar-binding SBPs may result from carbohydrate-mediated metabolic suppression (*52*). The third most abundant group comprises SBPs for ions (e.g., phosphate, sulfate, zinc),

which are needed in smaller quantities (*53*). The least abundant SBPs are those for vitamins and siderophores, substances required in minute amounts. These results demonstrate that, in addition to transporter-SBP interaction affinity, substrate demand also influences the abundances of SBPs.

Similar to the SBPs, the abundances of the NBDs exhibited substantial variation, ranging from approximately 2500 copies/cell (GlnQ, involved in glutamine uptake) to around 1 copy/cell (FecE, participating in Fe^{3+}-dicitrate uptake). Their abundance hierarchy was comparable (though not identical) to that of the SBPs, i.e., peptides/amino acids > ions > sugars > vitamins/siderophores (Figure 3A). The TMDs displayed an identical abundance hierarchy, but their estimated cellular numbers were considerably lower than those of the NBDs (Figure 3B), which may be interpreted to suggest a stoichiometric excess of the latter. However, we could not detect any substantial amount of the NBDs in the cytosolic fractions, where their abundance was similar to that of *bona fide* membrane proteins, suggesting that these remnants of "cytosolic" NBDs likely stem from incomplete removal of membrane fragments from the soluble fraction. As shown later the NBDs are membrane associated in a TMD-dependent manner. We therefore suggest that the apparent stoichiometric excess of the NBDs over the TMDs arises from the technical limitations of membrane protein quantification by $LC\text{-}MS^2$ (*54*, *55*).

SBP-transporter stoichiometries

Another clear trend that emerges concerns the SBP-transporter stoichiometry: In all the systems belonging to the Type-I subgroup of ABC importers (*6*, *56*), i.e., systems that import peptides, amino acids, and sugars, we observed the SBP in stoichiometric excess relative to the transporter (Figure 4A, open bars). Similar stoichiometric ratios have been deduced from measuring protein synthesis rates (*57*). In contrast, this ratio was reversed in all Type-II systems (systems that import siderophores and vitamins), and the transporter was found in stoichiometric excess relative to the SBP (Figure 4A, closed bars). We postulated that substrate availability may modulate SBP-transporter stoichiometries, where substrate presence either negatively or positively regulates component expression, thereby altering expression levels and stoichiometric ratios. To test this, we conducted experiments in the presence of various substrates. Our analysis focused on the Met, Mal, Yec, Cys, and Btu systems, which represent both Type-I and Type-II systems and span a spectrum of systems' abundances, ranging from high (Met), intermediate (Yec, Cys), and low (Mal) to very low (Btu). To ensure system saturation substrates were added at concentrations 5- to 10-fold higher than their SBP binding affinities (*58–61*). For the Met system, we tested two substrates: L-methionine and D-methionine. Both are recognized by the SBP (MetQ) and inhibit the ATPase activity of the transporter by binding to its cytoplasmic regulatory domain (*62*). However, the proteinogenic L-isomer is imported with much higher affinity the system (*44*). As shown in Figure 4B, the expression levels of the system's components, and consequently their stoichiometry, remained largely unaffected by both the

inhibitory and transported substrates. Similar results were observed for the Btu (Figure 4C) and Mal (Figure S7A) systems, where the expression levels of the system's components and their stoichiometry remained unchanged in the presence of the transported substrate. In our experiments with the Cys and Yec systems, we tested two related substrates: L-cysteine and its oxidized dimer derivative, L-cystine. Both substrates are recognized and imported by the Yec system and are linked to regulation of the expression of the Cys system (*43*, *61*, *63*). Our results showed that the expression levels of all three components—substrate-binding protein (SBP), nucleotide-binding domain (NBD), and transmembrane domain (TMD)—in both cysteine-related systems were markedly reduced in the presence of L-cysteine and L-cystine, with L-cystine exerting stronger repression (Figure S7B-C). Despite these changes in expression levels, the stoichiometric ratios between the components remained relatively constant, with the SBP-transporter stoichiometry in the Yec and Cys systems consistently greater than 1 (Figure S7B-C).

These findings suggest that, although there is some variability among different systems, the SBP-transporter stoichiometry is a robust parameter inherent to these systems and is not significantly affected by the presence or absence of substrate.

As shown in Figure 4A, in Type-II systems the the SBP-transporter stoichiometry << 1, and this ratio is substrate independent (Figure 4C). This is a very surprising observation that raises questions about the relevance of in vitro transport assays conducted with such systems, which assume that the SBP-transporter stoichiometric ratio is >>1 (*42*, *49*, *64–66*). At this point, we can only speculate about the forces that shaped the different SBP-transporter stoichiometries in Type-I and Type-II systems. Possibly, the higher interaction affinities between SBP and transporters in Type-II systems necessitated their reduced stoichiometry. Support for this idea is presented in the final results section of this report, which highlights the functional implications of this unexpected stoichiometry.

Interdependence of expression and membrane localization

When comparing whole-cell lysates to membrane fractions prepared from the same cells, we observed a 5-6-fold enrichment in the fractional abundances of the TMDs (see slope of the linear fit in Figure S1C). This enrichment factor is somewhat greater than the one expected based on the fraction of membrane proteins in *E. coli* (20-25%, (*67*)) and possibly reflects the non-monotonous technical improvement in detecting membrane proteins associated with reduced sample complexity (*68*). In contrast, the SBPs were heavily under-represented in the membrane fraction. This is not surprising given the stoichiometric mismatch between SBP and the transporter in type I systems and considering that the periplasm is discarded during membrane preparation. However, there were three exceptions to this trend, and the SBPs MetQ, BtuF, and FhuD were enriched in the membrane fraction (Figure 5). For MetQ, the SBP of the methionine import system, this is not surprising since MetQ is uncharacteristically tethered to

the membrane via a lipid anchor (*69*, *70*). BtuF and FhuD on the other hand are "regular" periplasmic proteins that do not contain a membrane anchoring domain. Nevertheless, FhuD and BtuF were not detected in the periplasm and were exclusively membrane-bound. This finding challenges the prevailing dogma that periplasmic diffusion of substrate-binding proteins (SBPs) is a fundamental aspect of the ABC transport mechanism.

The membrane association of BtuF and FhuD could be a result of a direct interaction with membrane lipids (as is the case of MetQ), a specific interaction with their cognate TMDs, or interactions with an unknown membrane protein(s). To distinguish between these possibilities, we repeated the experiments with strains carrying chromosomal deletions of the cognate TMDs of 8 different import systems. In terms of total expression levels, the SBPs were not deleteriously affected by the deletion of their cognate TMDs (Figure 6A). Notably, the expression of the SBPs for molybdate (ModA) and zinc (ZnuA) increased 20 and 30-fold (respectively) upon deletion of the corresponding TMDs. We suspect that this represents a substrate-specific starvation response. The cellular requirement both zinc and molybdate cannot be compensated for by alternative systems. In contrast, SBPs that were not induced by deletion of their TMDs are either of systems that can be complemented by alternative sugars/amino acids/peptides (*e.g.*, His, Mal, Yec, Met) or are not essential under these growth conditions (Fhu, Btu).

Next, we tested whether the membrane association of MetQ, BtuF, and FhuD depended on their interactions with cognate TMDs. Deletion of the TMD MetI had no effect on the membrane association of its cognate SBP, MetQ (Figure 6B). This result is unsurprising, as MetQ is the only *E. coli* SBP directly anchored to the membrane via covalent lipidation (*69*).

In contrast, the stable membrane association of BtuF and FhuD, both type-II system SBPs, was entirely dependent on the presence of cognate TMDs: Upon deletion of these TMDs, the cellular copy numbers of BtuF and FhuD remained unchanged (Figure 6A), but their membrane association was completely lost (Figure 6B), demonstrating that this localization was mediated through specific SBP-TMD interactions. This stable and specific association between SBPs and TMDs in type-II systems challenges the assumption that cyclic association-dissociation of SBPs is essential for transport by ABC importers.

To complement these studies, we performed membrane association biochemical assays. In these experiments we permeabilized the outer membrane of the cells by a mild osmotic shock treatment (see methods). We then added purified SBPs, incubated, and washed the cells. Our rational was that SBPs that freely diffuse in the periplasm will be removed by this wash step while those that are firmly membrane-associated will not. We tested two Type-I SBPs HisJ and FliY and observed that they were indeed removed by the wash step (Figure 6C-D), in line with the proteomics data that shows that SBPs of Type-I systems are not membrane associated. In contrast, and in line with the membrane enrichment observed for Type-II

SBPs (Figure 5), BtuF remained membrane-associated despite the wash step (Figure 6E). Also in line with the proteomics data was the finding that the membrane association of BtuF fully depended on the expression of its cognate TMDs (Figure 6E). These complementary biochemical studies further suggest that SBPs and TMDs in type-II systems associate very tightly, potentially remaining bound without dissociating.

Like the substrate-binding proteins (SBPs), the nucleotide-binding domains (NBDs) did not exhibit detrimental effects on total expression levels upon the deletion of their corresponding transmembrane domains (TMDs). Contrarily, the majority of NBDs demonstrated an increase in expression when their TMDs were absent (Figure 7A). The only exception was observed with MetN, which completely failed to express in the absence of MetI. This, coupled with the distinct membrane tethering of MetQ, indicates that the methionine system is an exceptional case. Despite the heightened expression levels, the NBDs could hardly be detected in the membrane fraction (Figure 7B). This implies that, while the NBDs do not necessitate their corresponding transmembrane domains (TMDs) for expression per se, they are absolutely dependent on them for membrane association.

Our collection of deletion strains included two transporters with heterodimeric TMDs: the histidine transporter $HisP_2QM$ and the maltose transporter $MalFGK_2$. The structures of $MalFGK_2$ (*71*) show that MalF and MalG are highly asymmetric, each contributing a different subset of residues to the translocation pore and to the interaction surface with the SBP. The consensus is therefore that this heterodimeric organization is an inherent and essential property of such transporters. To our great surprise, MalF was still present in the membranes of the Δ*malG* strain, and as if to compensate for the *malG* deletion, the amount of MalF increased almost exactly 2-fold (Figure S8A). In contrast, we could not detect MalG in the membranes of cells deleted of *malF* (not shown). These results suggest that MalF can insert into the membrane independently of MalG, and not *vice versa*. In line with these observations, the membrane association of MalK (the NBD of the maltose transporter) was hardly affected by the absence of MalG, but was nearly completely abolished in the absence of MalF, indicating that the expression of MalF is sufficient and essential for the membrane association/localization of MalK (Figure S8B). A somewhat similar phenomenon was observed with the histidine transporter HisPQM. Both HisM and HisQ (the TMDs) were detected in the absence of their counterpart. Of the two, HisQ was less dependent on HisM than *vice versa*, and its expression in the membranes of *ΔhisM* cells was ~5-fold higher than that of HisM in *ΔhisQ* cells (Figure S8C). Strikingly, HisP (the NBD) was readily detected in membranes devoid of HisM but was completely absent from those devoid of HisQ (Figure S8C). The above observations the raise the possibility that these heteromeric transporters may also form stable homomeric membrane-bound complexes (*i.e.*, $MalF_2K_2$ and $HisQ_2P_2$), a suggestion that requires further investigation.

Mechanistic implications of SBP-transporter stoichiometries

As shown in Figure 4, all Type-I systems exhibited a stoichiometric excess of the substrate-binding protein (SBP) in the range of 10-200-fold over the transporter. Notably, in the case of the Type-I maltose transporter, this surplus of the SBP has been established as crucial for activity. Mutations in the signal sequence of the SBP (MalE), which reduce its export to the periplasm and consequently lower its periplasmic copy number, lead to a decrease in transport rates. This reduction in transport rates results in impaired utilization of maltose as a carbon source (*72*, *73*). It appears, therefore, that in systems involved in the transport of abundantly available biomolecules, particularly those required in substantial quantities such as carbohydrates and amino acids, the stoichiometric excess of the SBP represents an essential mechanistic feature.

Surprisingly, and perhaps counterintuitively, Type-II systems exhibited a reversed ratio, with the transporter found in 10-100-fold stoichiometric excess over the substrate-binding protein (Figure 4A), and this stoichiometry persisted both in the presence and absence of substrate (Figure 4C).

To assess the implications of the 'reversed stoichiometry' observed in Type-II systems, we adjusted the SBP ratio in the Btu system by increasing the expression of the substrate-binding protein (SBP) (see methods for details). LC-MS^2 analysis confirmed that this adjustment, referred to as $BtuF_{high}$, replicates the SBP-transporter stoichiometric ratio observed in Type-I systems, characterized by an approximate 100-fold excess of SBP. Importantly, the only modification introduced was the alteration of this stoichiometric ratio, with all other mechanistic aspects of the Btu system remaining consistent with the wild-type system.

For these experiments, we utilized an *E. coli* strain that can synthesize methionine exclusively through vitamin B12-dependent catalysis (*42*). As a result, this strain can only grow in media supplemented with either methionine or vitamin B12. When vitamin B12 is provided, the high-affinity uptake activity of the BtuCD-F system becomes crucial for its growth.

In media supplemented with methionine, we observed no distinction between wild-type (WT) cells expressing the intrinsic low levels of BtuF (referred to as $BtuF_{low}$) and those expressing $BtuF_{high}$ (Figure 8A). Subsequently, we replicated these experiments but instead of methionine supplemented the media with a surplus of vitamin B12. As shown in Figure 8B, in the presence of high concentrations of vitamin B12 which support 100% growth (compare Figures 8A and 8B), the elevated expression of the substrate-binding protein (SBP) did not confer either a growth advantage or a disadvantage. Remarkably, as we lowered the concentrations of vitamin B12, making it limiting for growth, the $BtuF_{low}$ cells exhibited a substantial growth advantage, and this advantage became more pronounced as the concentrations decreased (Figure 8C-F). This stands in stark contrast to the observations for the model Type-I transporter MalFGK-E, where reduced substrate-binding protein (SBP) led to decreased transport and impaired growth (*72*, *73*).

A link between thermodynamics, conformational dynamics, copy number, and component stoichiometry

The unexpected phenomenon, where increasing amounts of one of the components of a system leads to reduced output, can be explained by considering the thermodynamics and physiological role of systems such as Btu.

The physiological role of such Type-II systems is to import scarce nutrients, requiring the substrate-binding protein (SBP) to have a very high binding affinity (*56*). For such high-affinity ligand binding, evolution has favored a lock-and-key mechanism: the ligand-binding site in the SBP is mostly pre-formed and undergoes minimal structural rearrangement upon ligand binding (Figure 9, left). As a result, the ligand-free and ligand-bound conformations of the SBP are similar (*74*, *75*). Consequently, the transporter cannot readily differentiate between the ligand-free and ligand-bound SBP, and under normal physiological concentrations both bind to it with high affinity ((*41*), Figure 9, left). This contrasts with Type-I systems, where a substantial conformational change in the SBP occurs upon ligand binding (*56*), allowing the transporter to distinguish between the ligand-free and ligand-bound forms (Figure 9, right).

Although the nutrients imported by Type-II systems are essential for growth, they are needed in small amounts. For example, as established in previous observations (*42*), and further corroborated by our findings (Figure 8B), as little as 5 nM vitamin B12 supports maximal growth.

This concentration corresponds to a periplasmic presence of approximately 3-4 vitamin B12 molecules, perfectly aligning with the cellular copy number of BtuF (4 copies/cell, Table S4). The cellular copy number of the transporter is approximately 20 (Table S4), leading to a SBP:transporter stoichiometry of <1 (Figure 10, upper left). Under these conditions, transporter docking sites are available for all vitamin B12-bound BtuF molecules and import is normal. In the manipulated system ($BtuF_{high}$), the SBP:transporter stoichiometry is >1 (Figure 10, upper right). Under these conditions, the expression of excess BtuF relative to vitamin B12 leads to the generation of a population of vitamin B12-free BtuF molecules. Previous studies have demonstrated that vitamin B12-free BtuF exhibits very high affinity towards its cognate transporter (*41*). Consequently, these ligand-free BtuF molecules will compete with the fewer ligand-bound ones for docking to the available transporters (Figure 10, upper right). Given their extremely slow dissociation rate ($\sim 10^{-7}$ S^{-1}, (*41*)) this will effectively clog the system and reduce uptake rates, as demonstrated in Figure 8C-F. A similar problem does not arise in Type-I systems (Figure 10, bottom panels). Their substrates are sufficiently abundant to saturate the SBPs, diminishing the competition between substrate-free and loaded SBPs (Figure 10, bottom right). In addition, Type-I transporters preferentially associate with substrate-loaded SBPs, and their SBPs rapidly dissociate from the transporters, avoiding the problem of clogging the transporters with substrate-free SBPs (*41*, *45–47*). As shown previously (*72*, *73*), low expression of Type-

I SBPs leads to reduced uptake (Figure 10, bottom left), in direct contrast to Type-II systems (Figure 10, upper left).

It therefore seems that two different SBP: transporter stoichiometries evolved, with ratios >1 and <1 tailored for acquiring biomolecules of high and low abundance, respectively.

How is expression regulated?

Interestingly, many import systems are expressed at significant levels even in the absence of their specific substrates in the growth medium (*e.g.*, Met, Liv, His; Figures 2 and 3). This observation suggests that many systems are constitutively expressed, remaining in a state of readiness for the appearance of their substrates. Such a strategy eliminates the need for the time-consuming processes of transcription, translation, membrane insertion, and complex assembly, which could result in missed import opportunities.

In cases where excessive import of the substrate is toxic (e.g., zinc, nickel), expression is tightly controlled by substrate-responsive transcriptional elements (*76*, *77*). However, the findings presented in Figures 4B-C and S7A suggest that direct substrate-mediated feedback regulation does not apply to certain systems, raising questions about the mechanisms governing their expression.

An alternative explanation could link expression to broader physiological states. For carbohydrate importers, expression might be tied to the cell's energetic balance. Similarly, for peptide and amino acid importers, the general availability of these nutrients could influence their expression levels. A comprehensive approach integrating multiple omics techniques—such as transcriptomics, proteomics, and metabolomics—could provide a holistic understanding of the factors driving the expression of these import systems.

Concluding remarks

We integrated proteomic analysis with functional assays to explore correlations between thermodynamic/kinetic properties, substrate specificity, copy number, and component stoichiometry in ABC import systems. Our findings reveal abundances that vary over 4-5 orders of magnitude and correlate with the quantities of nutrients requiring acquisition. Additionally, we observed that receptors (SBPs) of systems importing rare compounds do not freely diffuse in the periplasm but are firmly docked to their cognate membrane-embedded transporter. The tight association between type II SBPs and their cognate TMDs raises the possibility that transport in these systems may occur without the SBP ever dissociating. While this idea is intriguing, to the best of our knowledge, experimental evidence supporting its existence is still lacking. Notably, such systems utilize a "reversed" stoichiometry where the receptor is found in paucity relative to the transporter. Taken together, the results showcase correlations between

physiological roles, molecular-level attributes, and cellular-context parameters, suggesting their coevolution to optimize the output of multi-component systems.

Materials & Methods

Mass Spectrometry sample preparation and data analysis

Cultures of the *E. coli* K12 strain BW25113, the progenitor strain of the Keio clone collection (*29*), were grown to mid-exponential phase in M9 liquid media containing 42.2 mM Na_2HPO_4, 22.0 mM KH_2PO_4, 8.6 mM NaCl, 18.7 mM NH_4Cl, 1% thiamine, 1 mM MgSO4, 10 μM CaCl2, 0.025 % arginine, 0.025 % lysine, and 0.5 % glucose. Cells were harvested by centrifugation, washed in PBS and stored in -80°C. Where indicated, membranal, cytosolic, and periplasmic fractions were prepared from these cell pellets. For preparation of membrane fraction, cells were re-suspended in 50 mM Tris-HCl, pH 7.5, 0.5 M NaCl, and ruptured by tip sonication (3 × 20 s, 600 Watts). Debris and unbroken cells were removed by centrifugation (10 min, 10,000 × *g*) and the membranes were pelleted by ultracentrifugation at 120,000 × *g* for 45 min. The membranes were washed and re-suspended in 50 mM Tris-HCl, pH 7.5, 0.5 M NaCl and stored in -80°C. Where indicated, membranes were subjected to an additional wash step with 100mM sodium bicarbonate, 2 M sodium chloride, or 25 mM EDTA.

Next, the samples were dissolved in 10mM DTT 100mM Tris and 5% SDS, or 1 % DDM, 1% DM or a mixture of or 1% DDM + 1% DM, as indicated. Samples were sonicated and boiled in 95^0 C for 5 min and precipitated in 80% acetone. The protein pellets were dissolved in in 9M Urea and 400mM ammonium bicarbonate than reduced with 3mM DTT (60ºC for 30 min), modified with 10mM iodoacetamide in 100mM ammonium bicarbonate (room temperature 30 min in the dark) and digested overnight in 2M Urea, 25mM ammonium bicarbonate at 37°C using a 1:50 (mol/mol) of modified trypsin (Promega), 1:10 (mol/mol) Chymotrypsin(Roche), 1:50 (mol/mol) ProAlanase (Promega), 1:50 (mol/mol) WalP (Cell signaling technology), 1:3 (mol/mol) Pepsin (Promega), or 1:50 (mol/mol) Lys-C (Fujifilm), as indicated, and digestion was quenched by addition of 1% formic acid.

The peptides were desalted using C18 tips (Top tip, Glygen), dried and re-suspended in 0.1% Formic acid, and resolved by reverse-phase chromatography on 0.075 X 180-mm fused silica capillaries (J&W) packed with Reprosil reversed phase material (Dr Maisch GmbH, Germany). The peptides were eluted with linear gradients of acetonitrile with 0.1% formic acid in water: 120 minutes of 5 to 28%, 15 minutes of 28 to 95%, and 25 minutes at 95% at flow rates of 0.15 μl/min. Mass spectrometry was performed using a Q Exactive HFX mass spectrometer (Thermo) in a positive mode (m/z 300–1800, resolution 120,000 for MS1 and 15,000 for MS2) using repetitively full MS scan followed by collision induces dissociation (HCD, at 27 normalized collision energy) of the 18 most dominant ions (>1 charges) selected

from the first MS scan. The AGC settings were 3x106 for the full MS and 1x105 for the MS/MS scans. The intensity threshold for triggering MS/MS analysis was 1x104. A dynamic exclusion list was enabled with exclusion duration of 20 s.

Mass spectrometry data was analyzed using the MaxQuant software 1.5.2.8 (*78*) for peak picking and identification using the Andromeda search engine, searching against the human proteome from the Uniprot database with mass tolerance of 6 ppm for the precursor masses and 20 ppm for the fragment ions. Oxidation on methionine and protein N-terminus acetylation were accepted as variable modifications and carbamidomethyl on cysteine was accepted as static modifications. Minimal peptide length was set to six amino acids and a maximum of two miscleavages was allowed. The data was quantified by label free analysis using the same software. Peptide- and protein-level false discovery rates (FDRs) were filtered to 1% using the target-decoy strategy. Protein table were filtered to eliminate the identifications from the reverse database, and common contaminants and single peptide identifications Statistical analysis of the identification and quantization results was done using Perseus 1.6.10.43 software (*79*).

Calculation of cellular copy numbers

To calculate cellular copy numbers, equation 1 was used to determine relative iBAQ values (*36*, *37*) for each protein:

(1) $$riBAQ(i) = \frac{iBAQ(i)}{Total\ iBAQ\ (sample)}$$

where *riBAQ(i) is the* relative iBAQ value of protein *i*, *iBAQ(i)* is its iBAQ value as determined by MaxQuant, and *Total iBAQ (sample)* is the sum of all iBAQ values of the sample.

Using equation 2, the mass (in grams) was calculated for each protein by multiplying *riBAQ(i)* by the total protein mass of the sample:

(2) $$m\ (i) = riBAQ(i) \times Total\ mass\ (sample)$$

The total number of moles present in the sample for a given protein was obtained using equation 3,

(3)

$$n\ (i) = \frac{m(i)}{MW\ (i)}$$

where *n* is the total number of moles, *m* is the total mass of a given protein present in the sample, and *MW* is its molecular weight.

The total number of molecules of a given protein present in the sample, *N (i)*, was then obtained using Avogadro's number (equation 4).

$$N\ (i) = n\ (i) \times 6.023 \times 10^{23} \quad (4)$$

Finally, cellular copy numbers, *C(i)*, were determined using equation 5

$$C\ (i) = \frac{N(i)}{number\ of\ cells} \quad (5)$$

Where *N(i)* is the total number of molecules obtained using equation 4 and the number of cells determined by colony counting.

Quantification using purified proteins standards

MetQ, FliY, BtuF, MetN, YecS, BtuD, MetI, and YecC were purified to >90% homogeneity as previously described by our group (*41*, *43*). 5µg protein from each protein was digested by trypsin, following the method described above. To minimize technical variation, the proteins were combined in a mixture, containing 3.45×10^{-11} mols from each, and desalted. A mixture containing 3.45×10^{-12} mols from each protein was then analyzed by LC-MS^2 using a Thermo HFX mass spectrometer. Data were processed using MaxQuant 2.4 with a 1% FDR, and all proteins were identified by at least 6 peptides. The ratio between the measured intensity of each purified protein and its known molar amount was used to convert the intensity measured in whole-cell samples into molar quantities. This molar amount was then compared to the value calculated using iBAQ quantification.

Membrane association assays

For the membrane association studies only fresh cultures, ones that have not been frozen and/or stored, were used. The experiments were conducted essentially as previously described (*41*, *80*) with the following modifications. Cells were transformed with an empty vector or with the same vector encoding the transporters YecSC, HisPQM, or BtuCD, as indicated. Cultures were grown in LB-ampicillin medium at 37 °C with shaking to mid-exponential phase, and protein expression was induced by isopropyl β-D-1-thiogalactopyranoside (0.5 mM) for 1 hour. Cells were harvested and resuspended in 10 mM Tris·HCl, pH 7.5, and 0.75 M sucrose. The cell suspension was then incubated on ice for 20 min in the presence of

100 µg/mL lysozyme (Amresco) and 2 volumes of 1.5 mM EDTA. The spheroplasts were then stabilized by addition of 25 mM $MgCl_2$ and DNA originating form ruptured cells was digested with 100 µg/mL DNase-I (Worthington). The spheroplasts were pelleted and resuspended in 100 mM Tris·HCl, pH 7.5, 150 mM NaCl, and 5 mM $MgCl_2$ to an OD_{600} of about 10 and kept on ice until use. Purified FLAG-tagged SBPs were added to the spheroplasts suspension (160 nM BtuF, 5µM FliY, 15µM HisJ) and following a 10-min incubation, unbound material was removed by 5 min centrifugation at 2500 ×g. The amount of FLAG-tagged SBPs in the total, washed, and bound fractions was visualized using standard immuno-blot procedures, using an anti-FLAG M2 HRP-conjugate antibody (Sigma).

Vitamin B12 utilization assays

This assay is based on the original protocol developed by the Kadnar lab (*59*). In the *E. coli ΔmetE* strain methionine biosynthesis is solely catalyzed by MetH, a vitamin B12-dependent methionine synthase. In this strain growth is therefore dependent on the exogenous addition of either methionine or vitamin B12. When the latter is supplied, growth fully depends on the uptake function of BtuCD-F(*86*). In the experiments shown in Figure 8, $BtuF_{low}$ cells refer to *ΔmetE* cells transformed with an empty vector, and $BtuF_{high}$ cells refer to the same cells transformed with a BtuF-encoding vector. Expression of the plasmid was not induced during the experiment, and hence, excess BtuF in the $BtuF_{high}$ cells originates from promoter leakiness. As detailed in the text, this leaky expression amounts to 1000-2000 copies of BtuF per cell. Cultures were grown in LB media supplemented with 50 µg/mL kanamycin and 100 µg/mL ampicillin to mid log phase, washed and resuspended in Davis minimal media to OD_{600} of 0.05. Cultures (0.2 mL) were then grown in absence or presence of methionine or vitamin B12, as indicated. The optical density of the cultures was measured every 5 min for 12 h using an automated plate reader (Infinite M200 Pro; Tecan).

References

1. D. C. Rees, E. Johnson, O. Lewinson, ABC transporters: the power to change. *Nat. Rev. Mol. Cell Biol.* **10**, 218–227 (2009).

2. K. Kuchler, The ABC of ABCs: Multidrug resistance and genetic diseases. *FEBS J.* **278**, 3189 (2011).

3. A. Ersoy, B. Altintel, N. Livnat Levanon, N. Ben-Tal, T. Haliloglu, O. Lewinson, Computational analysis of long-range allosteric communications in CFTR. *eLife* **12** (2023).

4. C. A. McDevitt, A. D. Ogunniyi, E. Valkov, M. C. Lawrence, B. Kobe, A. G. McEwan, J. C. Paton, A Molecular Mechanism for Bacterial Susceptibility to Zinc. *PLoS Pathog* **7**, e1002357 (2011).

5. E. Vigonsky, I. Fish, N. Livnat-Levanon, E. Ovcharenko, N. Ben-Tal, O. Lewinson, Metal binding spectrum and model structure of the Bacillus anthracis virulence determinant MntA. *Met. Integr. Biometal Sci.* **7**, 1407–19 (2015).

6. G. H. Scheepers, J. A. Lycklama a Nijeholt, B. Poolman, An updated structural classification of substrate-binding proteins. *FEBS Lett.* **590**, 4393–4401 (2016).

7. J. R. Wiśniewski, H. Koepsell, A. Gizak, D. Rakus, Absolute protein quantification allows differentiation of cell-specific metabolic routes and functions. *Proteomics* **15**, 1316–1325 (2015).

8. I. Cima, R. Schiess, P. Wild, M. Kaelin, P. Schüffler, V. Lange, P. Picotti, R. Ossola, A. Templeton, O. Schubert, T. Fuchs, T. Leippold, S. Wyler, J. Zehetner, W. Jochum, J. Buhmann, T. Cerny, H. Moch, S. Gillessen, R. Aebersold, W. Krek, Cancer genetics-guided discovery of serum biomarker signatures for diagnosis and prognosis of prostate cancer. *Proc. Natl. Acad. Sci. U. S. A.* **108**, 3342–3347 (2011).

9. J. A. Schäfer, S. Bozkurt, J. B. Michaelis, K. Klann, C. Münch, Global mitochondrial protein import proteomics reveal distinct regulation by translation and translocation machinery. *Mol. Cell* **82**, 435-446.e7 (2022).

10. K. L. Hickey, S. Swarup, I. R. Smith, J. C. Paoli, E. Miguel Whelan, J. A. Paulo, J. W. Harper, Proteome census upon nutrient stress reveals Golgiphagy membrane receptors. *Nature* **623**, 167–174 (2023).

11. A. Schmidt, K. Kochanowski, S. Vedelaar, E. Ahrné, B. Volkmer, L. Callipo, K. Knoops, M. Bauer, R. Aebersold, M. Heinemann, The quantitative and condition-dependent Escherichia coli proteome. *Nat. Biotechnol.* **34**, 104–110 (2016).

12. D. Nanavati, M. Gucek, J. L. S. Milne, S. Subramaniam, S. P. Markey, Stoichiometry and absolute quantification of proteins with mass spectrometry using fluorescent and isotope-labeled concatenated peptide standards. *Mol. Cell. Proteomics* **7**, 442–447 (2008).

13. C. Schmidt, C. Lenz, M. Grote, R. Lührmann, H. Urlaub, Determination of protein stoichiometry within protein complexes using absolute quantification and multiple reaction monitoring. *Anal. Chem.* **82**, 2784–2796 (2010).

14. A. Wepf, T. Glatter, A. Schmidt, R. Aebersold, M. Gstaiger, Quantitative interaction proteomics using mass spectrometry. *Nat. Methods* **6**, 203–205 (2009).

15. K. C. Tsolis, A. Economou, Quantitative Proteomics of the E. coli Membranome. *Methods Enzymol.* **586**, 15–36 (2017).

16. K. Krug, A. Carpy, G. Behrends, K. Matic, N. C. Soares, B. Macek, Deep coverage of the escherichia coli proteome enables the assessment of false discovery rates in simple proteogenomic experiments. *Mol. Cell. Proteomics* **12**, 3420–3430 (2013).

17. J. N. Adkins, H. M. Mottaz, A. D. Norbeck, J. K. Gustin, J. Rue, T. R. W. Clauss, S. O. Purvine, K. D. Rodland, F. Heffron, R. D. Smith, Analysis of the Salmonella typhimurium proteome through environmental response toward infectious conditions. *Mol. Cell. Proteomics MCP* **5**, 1450–1461 (2006).

18. B. K. Chi, K. Gronau, U. Mäder, B. Hessling, D. Becher, H. Antelmann, S-bacillithiolation protects against hypochlorite stress in Bacillus subtilis as revealed by transcriptomics and redox proteomics. *Mol. Cell. Proteomics MCP* **10** (2011).

19. Z. M. Al-Majdoub, B. Achour, N. Couto, M. Howard, Y. Elmorsi, D. Scotcher, S. Alrubia, E. El-Khateeb, A.-M. Vasilogianni, N. Alohali, S. Neuhoff, L. Schmitt, A. Rostami-Hodjegan, J. Barber, Mass spectrometry-based abundance atlas of ABC transporters in human liver, gut, kidney, brain and skin. *FEBS Lett.* **594**, 4134–4150 (2020).

20. Z. M. Al-Majdoub, H. Al Feteisi, B. Achour, S. Warwood, S. Neuhoff, A. Rostami-Hodjegan, J. Barber, Proteomic Quantification of Human Blood-Brain Barrier SLC and ABC Transporters in Healthy Individuals and Dementia Patients. *Mol. Pharm.* **16**, 1220–1233 (2019).

21. J. Wissing, L. Jänsch, M. Nimtz, G. Dieterich, R. Hornberger, G. Kéri, J. Wehland, H. Daub, Proteomics analysis of protein kinases by target class-selective prefractionation and tandem mass spectrometry. *Mol. Cell. Proteomics MCP* **6**, 537–547 (2007).

22. B. Fabre, T. Lambour, L. Garrigues, M. Ducoux-Petit, F. Amalric, B. Monsarrat, O. Burlet-Schiltz, M. P. Bousquet-Dubouch, Label-free quantitative proteomics reveals the dynamics of proteasome complexes composition and stoichiometry in a wide range of human cell lines. *J. Proteome Res.* **13**, 3027–3037 (2014).

23. M. A. Gillespie, C. G. Palii, D. Sanchez-Taltavull, P. Shannon, W. J. R. Longabaugh, D. J. Downes, K. Sivaraman, H. M. Espinoza, J. R. Hughes, N. D. Price, T. J. Perkins, J. A. Ranish, M. Brand, Absolute Quantification of Transcription Factors Reveals Principles of Gene Regulation in Erythropoiesis. *Mol. Cell* **78**, 960-974.e11 (2020).

24. N. M. Clarka, A. P. Fishera, B. Berckmansc, L. Van Den Broeck, E. C. Nelsona, T. T. Nguyena, E. Bustillo-Avendañod, S. G. Zebelle, M. A. Moreno-Risuenod, R. Simonc, K. L. Gallagherh, R. Sozzania, Protein complex stoichiometry and expression dynamics of transcription factors modulate stem cell division. *Proc. Natl. Acad. Sci. U. S. A.* **117**, 15332–15342 (2020).

25. P. Mehta, G. Jovanovic, T. Lenn, A. Bruckbauer, C. Engl, L. Ying, M. Buck, Dynamics and stoichiometry of a regulated enhancer-binding protein in live Escherichia coli cells. *Nat. Commun.* **4** (2013).

26. The EcoCyc Database (2023) | EcoSal Plus. https://journals.asm.org/doi/10.1128/ecosalplus.esp-0002-2023.

27. L. Arike, K. Valgepea, L. Peil, R. Nahku, K. Adamberg, R. Vilu, Comparison and applications of label-free absolute proteome quantification methods on Escherichia coli. *J. Proteomics* **75**, 5437–5448 (2012).

28. J. C. Wright, M. O. Collins, L. Yu, L. Käll, M. Brosch, J. S. Choudhary, Enhanced peptide identification by electron transfer dissociation using an improved mascot percolator. *Mol. Cell. Proteomics* **11**, 478–491 (2012).

29. T. Baba, T. Ara, M. Hasegawa, Y. Takai, Y. Okumura, M. Baba, K. A. Datsenko, M. Tomita, B. L. Wanner, H. Mori, Construction of Escherichia coli K-12 in-frame, single-gene knockout mutants: The Keio collection. *Mol. Syst. Biol.* **2** (2006).

30. H. MJ, L. SY, The Escherichia coli proteome: past, present, and future prospects. *Microbiol. Mol. Biol. Rev. MMBR* **70** (2006).

31. H. Song, N. Lou, J. Liu, H. Xiang, D. Shang, Label-free quantitative proteomic analysis of the inhibition effect of Lactobacillus rhamnosus GG on Escherichia coli biofilm formation in co-culture. *Proteome Sci.* **19** (2021).

32. J. H. Weiner, L. Li, Proteome of the Escherichia coli envelope and technological challenges in membrane proteome analysis. *Biochim. Biophys. Acta - Biomembr.* **1778**, 1698–1713 (2008).

33. X. Zhang, Less is more: Membrane protein digestion beyond urea-trypsin solution for next-level proteomics. *Mol. Cell. Proteomics* **14**, 2441–2453 (2015).

34. D. Samodova, C. M. Hosfield, C. N. Cramer, M. V. Giuli, E. Cappellini, G. Franciosa, M. M. Rosenblatt, C. D. Kelstrup, J. V. Olsen, ProAlanase is an Effective Alternative to Trypsin for Proteomics Applications and Disulfide Bond Mapping. *Mol. Cell. Proteomics* **19**, 2139–2156 (2020).

35. J. G. Meyer, S. Kim, D. A. Maltby, M. Ghassemian, N. Bandeira, E. A. Komives, Expanding proteome coverage with orthogonal-specificity α-lytic proteases. *Mol. Cell. Proteomics* **13**, 823–835 (2014).

36. J. B. Shin, J. F. Krey, A. Hassan, Z. Metlagel, A. N. Tauscher, J. M. Pagana, N. E. Sherman, E. D. Jeffery, K. J. Spinelli, H. Zhao, P. A. Wilmarth, D. Choi, L. L. David, M. Auer, P. G. Barr-Gillespie, Molecular architecture of the chick vestibular hair bundle. *Nat. Neurosci.* **16**, 365–374 (2013).

37. J. F. Krey, P. A. Wilmarth, J. B. Shin, J. Klimek, N. E. Sherman, E. D. Jeffery, D. Choi, L. L. David, P. G. Barr-Gillespie, Accurate label-free protein quantitation with high- and low-resolution mass spectrometers. *J. Proteome Res.* **13**, 1034–1044 (2014).

38. J. L. Radzikowski, S. Vedelaar, D. Siegel, Á. D. Ortega, A. Schmidt, M. Heinemann, Bacterial persistence is an active σS stress response to metabolic flux limitation. *Mol. Syst. Biol.* **12**, 882 (2016).

39. K. Valgepea, K. Adamberg, A. Seiman, R. Vilu, Escherichia coli achieves faster growth by increasing catalytic and translation rates of proteins. *Mol. Biosyst.* **9**, 2344–2358 (2013).

40. B. Soufi, K. Krug, A. Harst, B. Macek, Characterization of the E. coli proteome and its modifications during growth and ethanol stress. *Front. Microbiol.* **6** (2015).

41. O. Lewinson, A. T. Lee, K. P. Locher, D. C. Rees, A distinct mechanism for the ABC transporter BtuCD-F revealed by the dynamics of complex formation. *Nat. Struct. Mol. Biol.* **17**, 332–338 (2010).

42. N. Tal, E. Ovcharenko, O. Lewinson, A single intact ATPase site of the ABC transporter BtuCD drives 5% transport activity yet supports full in vivo vitamin B12 utilization. *Proc. Natl. Acad. Sci. U. S. A.* **110**, 5434–9 (2013).

43. S. Sabrialabe, J. G. Yang, O. Lewinson, Substrate recognition and ATPase activity of the E. coli cysteine/cystine ABC transporter YecSC-FliY. *J Biol Chem* (2020).

44. P. T. Nguyen, J. Y. Lai, A. T. Lee, J. T. Kaiser, D. C. Rees, Noncanonical role for the binding protein in substrate uptake by the MetNI methionine ATP Binding Cassette (ABC) transporter. *Proc. Natl. Acad. Sci.* **115**, E10596–E10604 (2018).

45. G. F. Ames, C. E. Liu, A. K. Joshi, K. Nikaido, Liganded and unliganded receptors interact with equal affinity with the membrane complex of periplasmic permeases, a subfamily of traffic ATPases. *J. Biol. Chem.* **271**, 14264–70 (1996).

46. M. K. Doeven, G. van den Bogaart, V. Krasnikov, B. Poolman, Probing receptor-translocator interactions in the oligopeptide ABC transporter by fluorescence correlation spectroscopy. *Biophys. J.* **94**, 3956–65 (2008).

47. E. Vigonsky, E. Ovcharenko, O. Lewinson, Two molybdate/tungstate ABC transporters that interact very differently with their substrate binding proteins. *Proc. Natl. Acad. Sci. U. S. A.* **110**, 5440–5 (2013).

48. M. R. Rohrbach, V. Braun, W. Köster, Ferrichrome transport in Escherichia coli K-12: altered substrate specificity of mutated periplasmic FhuD and interaction of FhuD with the integral membrane protein FhuB. *J. Bacteriol.* **177**, 7186–93 (1995).

49. J.-S. Woo, A. Zeltina, B. A. Goetz, K. P. Locher, X-ray structure of the Yersinia pestis heme transporter HmuUV. *Nat. Struct. Mol. Biol.* **19**, 1310–5 (2012).

50. B. D. Bennett, E. H. Kimball, M. Gao, R. Osterhout, S. J. Van Dien, J. D. Rabinowitz, Absolute metabolite concentrations and implied enzyme active site occupancy in Escherichia coli. *Nat. Chem. Biol.* **5**, 593–9 (2009).

51. X. P. Hu, H. Dourado, P. Schubert, M. J. Lercher, The protein translation machinery is expressed for maximal efficiency in Escherichia coli. *Nat. Commun.* **11** (2020).

52. B. Görke, J. Stülke, Carbon catabolite repression in bacteria: Many ways to make the most out of nutrients. *Nat. Rev. Microbiol.* **6**, 613–624 (2008).

53. R. Milo, P. Jorgensen, U. Moran, G. Weber, M. Springer, BioNumbers The database of key numbers in molecular and cell biology. *Nucleic Acids Res.* **38**, D750–D753 (2009).

54. C. C. Wu, J. R. Yates, The application of mass spectrometry to membrane proteomics. *Nat. Biotechnol.* **21**, 262–267 (2003).

55. N. Solis, S. J. Cordwell, Current methodologies for proteomics of bacterial surface-exposed and cell envelope proteins. *Proteomics* **11**, 3169–3189 (2011).

56. O. Lewinson, N. Livnat-Levanon, Mechanism of Action of ABC Importers: Conservation, Divergence, and Physiological Adaptations. *J. Mol. Biol.*, doi: 10.1016/j.jmb.2017.01.010 (2017).

57. G. W. Li, D. Burkhardt, C. Gross, J. S. Weissman, Quantifying absolute protein synthesis rates reveals principles underlying allocation of cellular resources. *Cell* **157**, 624–635 (2014).

58. R. J. Kadner, Transport systems for L-methionine in Escherichia coli. *J. Bacteriol.* **117**, 232–41 (1974).

59. N. Cadieux, C. Bradbeer, E. Reeger-Schneider, W. Köster, A. K. Mohanty, M. C. Wiener, R. J. Kadner, Identification of the periplasmic cobalamin-binding protein BtuF of Escherichia coli. *J. Bacteriol.* **184**, 706–17 (2002).

60. F. A. Quiocho, J. C. Spurlino, L. E. Rodseth, Extensive features of tight oligosaccharide binding revealed in high-resolution structures of the maltodextrin transport/chemosensory receptor. *Struct. Lond. Engl. 1993* **5**, 997–1015 (1997).

61. I. Ohtsu, N. Wiriyathanawudhiwong, S. Morigasaki, T. Nakatani, H. Kadokura, H. Takagi, The L-cysteine/L-cystine shuttle system provides reducing equivalents to the periplasm in Escherichia coli. *J. Biol. Chem.* **285**, 17479–17487 (2010).

62. N. S. Kadaba, J. T. Kaiser, E. Johnson, A. Lee, D. C. Rees, The high-affinity E. coli methionine ABC transporter: structure and allosteric regulation. *Science* **321**, 250–3 (2008).

63. A. Sirko, M. Zatyka, E. Sadowy, D. Hulanicka, Sulfate and thiosulfate transport in Escherichia coli K-12: evidence for a functional overlapping of sulfate- and thiosulfate-binding proteins. *J. Bacteriol.* **177**, 4134–4136 (1995).

64. E. L. Borths, B. Poolman, R. N. Hvorup, K. P. Locher, D. C. Rees, In vitro functional characterization of BtuCD-F, the Escherichia coli ABC transporter for vitamin B12 uptake. *Biochemistry* **44**, 16301–9 (2005).

65. M. Yang, N. Livnat Levanon, B. Acar, B. Aykac Fas, G. Masrati, J. Rose, N. Ben-Tal, T. Haliloglu, Y. Zhao, O. Lewinson, Single-molecule probing of the conformational homogeneity of the ABC transporter BtuCD. *Nat. Chem. Biol.* **14**, 715–722 (2018).

66. N. Livnat-Levanon, A. I Gilson, N. Ben-Tal, O. Lewinson, The uncoupled ATPase activity of the ABC transporter BtuC2D2 leads to a hysteretic conformational change, conformational memory, and improved activity. *Sci. Rep.* **6**, 21696 (2016).

67. T. Kalwarczyk, M. Tabaka, R. Holyst, Biologistics-Diffusion coefficients for complete proteome of Escherichia coli. *Bioinformatics* **28**, 2971–2978 (2012).

68. J. Alfonso-Garrido, E. Garcia-Calvo, J. L. Luque-Garcia, Sample preparation strategies for improving the identification of membrane proteins by mass spectrometry. *Anal. Bioanal. Chem.* **407**, 4893–4905 (2015).

69. C. Merlin, G. Gardiner, S. Durand, M. Masters, The Escherichia coli metD locus encodes an ABC transporter which includes Abc (MetN), YaeE (MetI), and YaeC (MetQ). *J. Bacteriol.* **184**, 5513–5517 (2002).

70. M. L. Carlson, R. G. Stacey, J. W. Young, I. S. Wason, Z. Zhao, D. G. Rattray, N. Scott, C. H. Kerr, M. Babu, L. J. Foster, F. D. Van Hoa, Profiling the Escherichia coli membrane protein interactome captured in peptidisc libraries. *eLife* **8** (2019).

71. M. L. Oldham, J. Chen, Snapshots of the maltose transporter during ATP hydrolysis. *Proc Natl Acad Sci U A* **108**, 15152–15156 (2011).

72. R. Manson M D, Boos W, Bassford JP Jr, Dependence of maltose transport and chemotaxis on the amount of maltose-binding protein - PubMed. *J Biol Chem* **15;260(17)** (1985).

73. H. Bedouelle, P. J. Bassford, A. V. Fowler, I. Zabin, J. Beckwith, M. Hofnung, Mutations which alter the function of the signal sequence of the maltose binding protein of Escherichia coli. *Nature* **285**, 78–81 (1980).

74. E. L. Borths, K. P. Locher, A. T. Lee, D. C. Rees, The structure of Escherichia coli BtuF and binding to its cognate ATP binding cassette transporter. *Proc. Natl. Acad. Sci. U. S. A.* **99**, 16642–7 (2002).

75. N. K. Karpowich, H. H. Huang, P. C. Smith, J. F. Hunt, Crystal structures of the BtuF periplasmic-binding protein for vitamin B12 suggest a functionally important reduction in protein mobility upon ligand binding. *J Biol Chem* **278**, 8429–8434 (2003).

76. S. I. Patzer, K. Hantke, The zinc-responsive regulator Zur and its control of the znu gene cluster encoding the ZnuABC zinc uptake system in Escherichia coli. *J. Biol. Chem.* **275**, 24321–24332 (2000).

77. K. De Pina, V. Desjardin, M. A. Mandrand-Berthelot, G. Giordano, L. F. Wu, Isolation and characterization of the nikR gene encoding a nickel-responsive regulator in Escherichia coli. *J. Bacteriol.* **181**, 670–674 (1999).

78. J. Cox, M. Mann, MaxQuant enables high peptide identification rates, individualized p.p.b.-range mass accuracies and proteome-wide protein quantification. *Nat. Biotechnol.* **26**, 1367–1372 (2008).

79. S. Tyanova, T. Temu, P. Sinitcyn, A. Carlson, M. Y. Hein, T. Geiger, M. Mann, J. Cox, The Perseus computational platform for comprehensive analysis of (prote)omics data. *Nat. Methods* **13**, 731–740 (2016).

80. H. Qasem-Abdullah, M. Perach, N. Livnat-Levanon, O. Lewinson, ATP binding and hydrolysis disrupt the high-affinity interaction between the heme ABC transporter HmuUV and its cognate substrate-binding protein. *J. Biol. Chem.* **292**, 14617–14624 (2017).

Acknowledgements

Funding

This work was supported by grants from NATO Science for Peace and Security Program (SPS project G5685), and the Israeli Academy of Sciences project 1006/18.

All data needed to evaluate the conclusions in the paper are present in the paper and/or the Supplementary Materials. Figures 9 and 10 were created with BioRender.com

Author contribution

Conceptualization: O.L., Methodology: H.A.Q, M.P., M.G., N.L.L., T.Z., O.L.,

Investigation: H.A.Q, M.P., M.G., N.L.L., T.Z., O.L., Analysis: H.A.Q, M.P., T.Z., O.L.,

Writing, review and editing: H.A.Q, M.P., M.G., N.L.L., T.Z., O.L.,

Competing Interests

The authors declare that they have no competing interests.

Data and materials availability

All data needed to evaluate the conclusions in the paper are present in the paper and/or the Supplementary Materials. Additional data related to this paper may be requested from the authors.

Figure legends

Figure 1. High correlation between iBAQ quantification of whole cells lysates and intensity-based quantification of purified proteins. 3.45 picomoles of each of the indicated proteins was trypsinized and analyzed by LC-MS^2 as detailed in the methods section. The intensity obtained for each of the purified proteins was then used to derive its "conversion factor", which is the ratio between the (known) mol amount of a given protein and its measured intensity. This conversion factor was then used to multiply the intensity values obtained for each protein in the whole cell samples, generating a predicted mol amount that is the product of the intensity score determined in whole cells and the conversion factor determined for the purified proteins. Shown is the correlation between the amount of mols determined using the iBAQ approach in whole cells and the amount of mols calculated using the intensities measured in whole cell multiplied by the "conversion factor" determined using the purified proteins (y-ordinate). The dashed line represents the linear fit, and the coefficient of determination (R^2) is indicated.

Figure 2: Abundances and correlations of the SBPs. Shown are the cellular copy numbers of 37 substrate binding proteins (SBPs), color coded as indicated according to their substrate group. Results are means of biological triplicates and error bars represent standard deviations (A). Shown are the correlations between the periplasmic concentrations of the SBPs and their substrate binding affinities (B) or their affinity towards cognate transporters (C). The dashed lines represent the linear fit, and the coefficient of determination (R^2) is indicated.

Figure 3. Cellular abundances of the Nucleotide Binding and Transmembrane Domains. Shown are the cellular copy numbers of 30 NBDs (A) and 37 TMDs (B), color coded as indicated according to their substrate group. Results are means of biological triplicates and error bars represent standard deviations.

Figure 4. Different SBP: transporter stoichiometries in Type I and II systems. Shown are representative SBP-transporter stoichiometries determined for Type I (open bars) and II systems (full bars). Results are means of biological triplicates and error bars represent standard deviations (A). Shown is the label-free quantification (LFQ) of the abundances of the components (SBP-blue, NBD-orange, TMD-grey) of the Met (B) and Btu (C) systems determined for cells grown in minimal media in the absence ("no addition") or presence of 20 μM D-methionine, 1 nM L-methionine, or 50 nM vitamin B12, as indicated. These concentrations correspond to 5-10-fold excess relative to the substrate binding affinities of the SBPs (45, 60). Results are means of biological triplicates and error bars represent standard deviations.

Figure 5. SBPs of Type-II systems are membrane bound. Shown (in Log2 scale) are the ratios between the abundances of the SBPs in whole cell lysates vs. their abundances in the membrane fraction. Results are means of biological triplicates and error bars represent standard deviations.

Figure 6. Co-localization of SBPs and TMDs in Type-II Systems. (A-B) Shown is the fold change in the abundances of the indicated SBPs following deletion of their cognate TMDs measured in total cell lysates (A) and membrane fractions (B). Shown are fold changes Error bars represent standard deviations, and results represent the mean of biological triplicates.
(C-E): Cells deleted of the indicated TMDs were transformed with an empty plasmid or one harboring the deleted TMD (-, +, as indicated). Cells were then permeabilized by mild osmotic shock and purified SBPs were added at concentrations x10 their K_D of interaction with their cognate transporters. Following a 15-min incubation, bound and unbound SBPs were separated by a wash step. Shown are immunoblots of SDS-PAGE of the total, washed, and cell-bound fractions for the Type-I systems Yec (C) and His (D) and for the Type-II system Btu (E). For the Btu system, an additional negative control was provided by cells that expressed the R56A mutant of BtuC which does not interact with BtuF.

Figure 7. TMD-dependent expression and membrane localization of the NBDs. Shown is the fold change in the total expression level (i.e., abundance determined in whole cell extracts) of the indicated NBDs upon deletion of their cognate TMDs (A). Shown is the membrane enrichment factor of the indicated NBDs measured in WT (full bars) or ΔTMD cells (open bars) (B). Error bars represent standard deviations, and results represent the mean of biological triplicates.

Figure 8. Unexpected advantage of SBP-Transporter stoichiometry < 1. *ΔmetE* cells rely on vitamin B12-dependent enzymatic methionine synthesis. Cell growth is contingent on exogenous methionine or vitamin B12, with BtuCD-F facilitating the import of the latter (27, 87). *ΔmetE* cells were cultured with the indicated additives, and the growth of cells with natural ($BtuF_{low}$, blue curves) and elevated ($BtuF_{high}$, red curves) BtuF levels is shown. In panel F, the ratio of the maximal growth rate between $BtuF_{low}$ and $BtuF_{high}$ cells is presented as a function of vitamin B12 concentrations. Notably, under vitamin B12 limitation, $BtuF_{low}$ cells exhibit approximately six-fold faster growth than $BtuF_{high}$ cells; under vitamin B12 abundance, growth is identical. Results are averages of biological triplicates, with error bars indicating standard deviations.

Figure 9. Different modes of ligand binding by Type-I and Type-II SBPs. Type-II SBPs (left) undergo minimal structural rearrangement upon ligand binding. As a result, the transporter cannot readily distinguish between the ligand-free and ligand-bound forms of the SBP, and both bind to it with high affinity. In contrast, Type-I SBPs (right) undergo significant structural rearrangement following ligand binding, and the transporter preferentially interacts with the ligand-bound form.

Figure 10. SBP-transporter stoichiometries < 1 are adapted to transporting scarce nutrients. Type-II systems, which import scarce compounds such as vitamins, function optimally when the SBP is present in stoichiometric paucity relative to the transporter (upper left). Due to the limited environmental availability of ligands, an excess of SBP leads to a large population of ligand-free SBPs that compete with ligand-bound ones for transporter interaction, resulting in reduced uptake (upper right).
In contrast, Type-I systems, which import abundant compounds like amino acids, perform best when the SBP is in stoichiometric excess relative to the transporter (bottom right). In these systems, excess SBP does not pose an issue because the transporter-SBP complex is inherently unstable, and the transporter preferentially interacts with substrate-loaded SBPs. However, in Type-I systems, a paucity of SBP results in fewer ligand-binding events, fewer successful transporter-SBP interactions, and reduced import (bottom left).

Supplementary legends

Supplementary Table S1. Composition of the ABC import systems in *E. coli* BW25113, based on the EcoCyc database (29)**.**

Supplementary Table S2. Shown are the different sample preparation protocols used, indicating strain (WT or deletion mutants), cellular fraction (where applicable), detergent, and protease. The components of the 'ABC importome' identified in each experiment are indicated by √ or **-**

Supplementary Table S3. Determination of absolute copy numbers using purified standards. 3.45 picomoles of each of the indicated proteins was trypsinized and analyzed by LC-MS/MS as detailed in the methods section. The iBAQ score obtained for each of the purified proteins was then used to derive its "Conversion factor", which is the ratio between the (known) mol amount of a given protein and its iBAQ value (A). This conversion factor was then used to multiply the iBAQ values obtained for each protein in the whole cell samples (B), generating a predicted mol amount that is the product of the iBAQ score determined in whole cells and the conversion factor determined using the purified proteins. For clarity of representation, these values were converted to LOG (10) scale and used to generate the scatter plot shown in Figure 1.

Supplementary Table S4. The complied dataset of the components of the 'ABC importome' identified in this study. Results are means of at least three biological replicates.

Supplementary Figure S1. Examples of high correlation between different datasets. Shown are the correlations between the iBAQ values obtained for two technical replicates (A), two technical biological replicates (B), for whole cells and membranes fractions (C), and for membranes before or after washing with 100 mM sodium carbonate (D). Also shown are the linear regressions (dashed black lines), their slopes, and the coefficients of determination (R^2).

Supplementary Figure S2. Low correlation between samples digested with different proteases. Shown are the correlations between the iBAQ values obtained for samples digested with either trypsin or chemotrypsin (A), digested with either trypsin or LysC (B), digested with either trypsin or pepsin (C), and digested with either trypsin or Proanalase (D). Also shown are the linear regressions (dashed black lines), their slopes, and the coefficients of determination (R^2).

Supplementary Figure S3. Low correlations between samples extracted with different detergents. Shown are the correlations between the iBAQ values obtained for samples extracted with either sodium dodecyl sulfate (SDS) or n-dodecyl β-D-maltoside (DDM) (A), SDS or n-decyl β-D-maltoside DM (B), and SDS or a mixture of DDM+DM (C). Also shown are the linear regressions (dashed black lines), their slopes, and the coefficients of determination (R^2).

Supplementary Figure S4. A comparison between the cellular copy numbers of SBPs determined in this study and in four other studies. Shown are the correlations between the copy number of the SBPs determined in this study and (14, 41-43) (D). Also shown are the linear regressions (dashed black lines) and the coefficients of determination (R^2).

Supplementary Figure S5. A comparison between the cellular copy numbers of SBPs determined by four other studies. Shown are the correlations between the copy number of the SBPs determined in in the studies of (14, 41-43) as indicated. Also shown are the linear regressions (dashed black lines) and the coefficients of determination (R^2).

Supplementary Figure S6. A comparison between trypsin and chymotrypsin. Shown are the cellular copy numbers of substrate binding proteins (SBPs), color coded as indicated according to their substrate group, determined by using trypsin (full bars) or chymotrypsin (open bars). Results are means of biological triplicates and error bars represent standard deviations (A). Shown are the correlations between the periplasmic concentrations of the SBPs, determined by using chymotrypsin, and their affinity towards cognate transporters (B). The dashed lines represent the linear fit, and the coefficient of determination (R^2) is indicated.

Supplementary Figure S7. SBP-transporter stoichiometries in the absence and presence of substrates. Shown is the label-free quantification (LFQ) of the abundances of the components (SBP-blue, NBD-orange, TMD-grey) of the Mal (A), Yec (B), or Cys (C) systems determined for cells grown in minimal media in the absence ("no addition") or presence of 15 μM D-maltose, 75 μM L-cysteine, or 50 μM L-cystine, as indicated. These concentrations correspond to 5-10-fold excess relative to the substrate binding affinities of the SBPs (44, 61, 62). Results are means of biological triplicates and error bars represent standard deviations.

Supplementary Figure S8. Asymmetric biogenesis of heteromeric systems. Shown are the membrane fraction abundances of MalF in WT and *ΔmalG* cells (A), of MalK in WT, *ΔmalF*, and *ΔmalG* cells (B), and of HisP, HisM, and HisP (as color coded) in WT, *ΔhisQ*, and *ΔhisM* cells (C). Results are means of biological triplicates and error bars represent standard deviations.

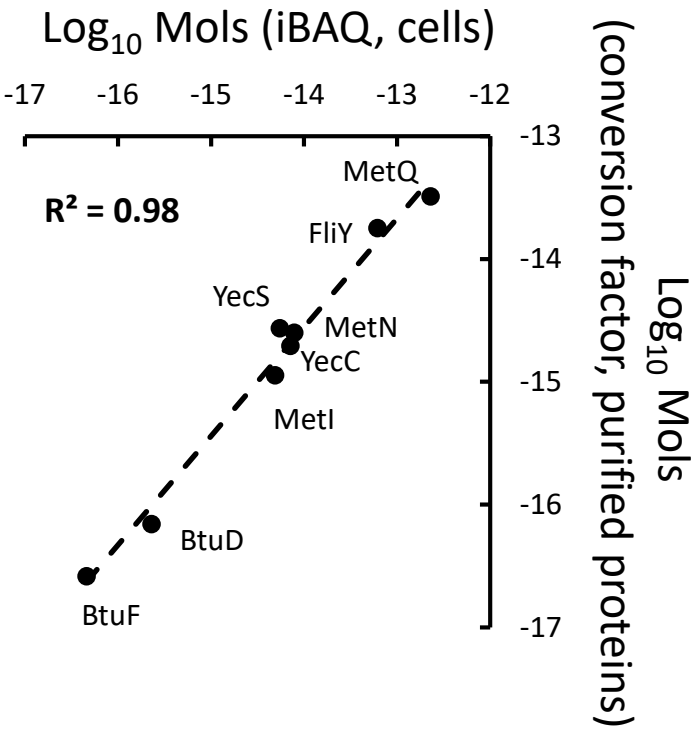
Log10 Mols (iBAQ, cells)
-17
-16
-15
-14
-13
-12
-13
-14
-15
-16
-17
Log10 Mols
(conversion factor, purified proteins)
R² = 0.98
MetQ
FliY
YecS
MetN
YecC
MetI
BtuD
BtuF

Figure 1

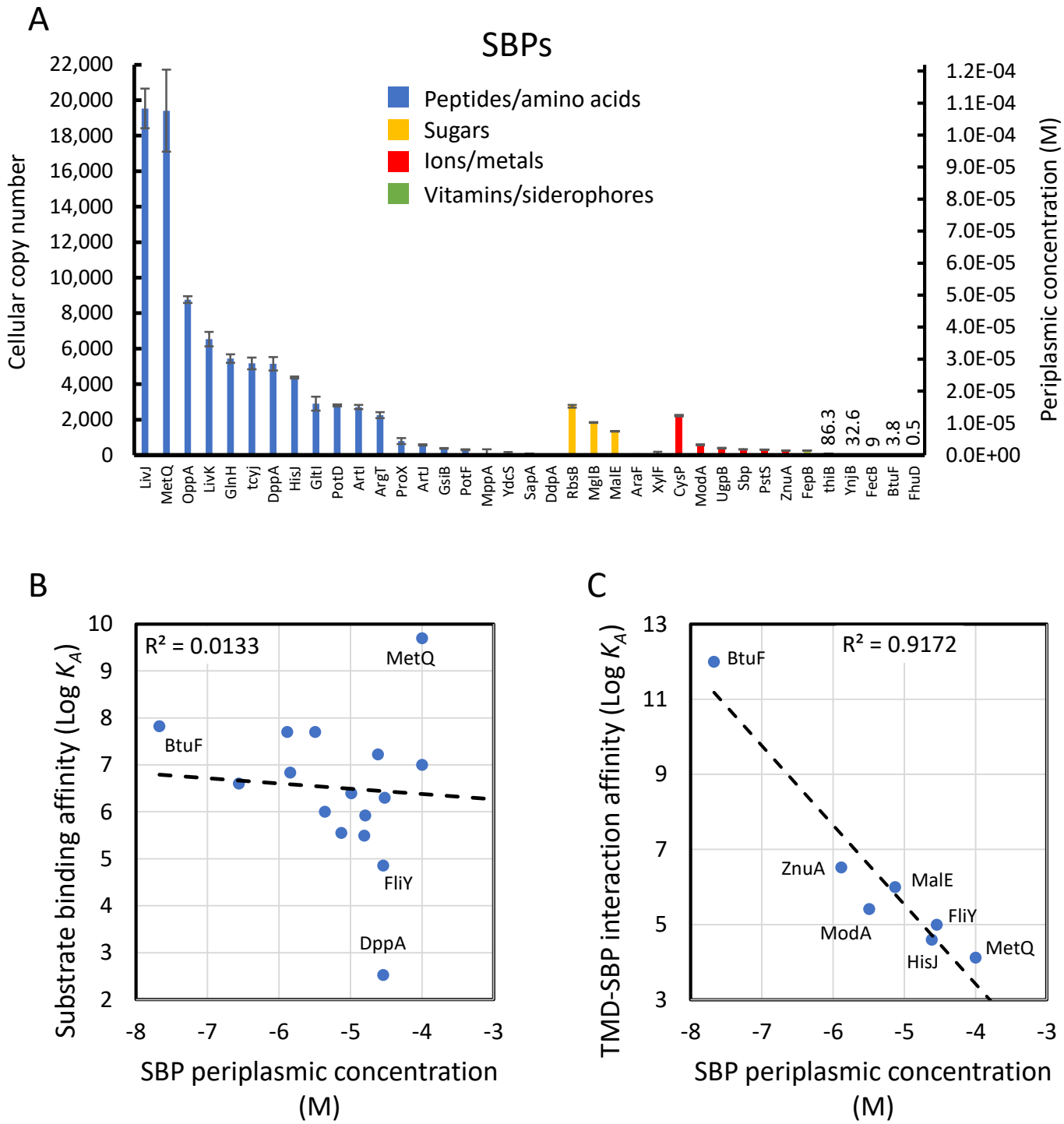
A
SBPs
Peptides/amino acids
Sugars
Ions/metals
Vitamins/siderophores
Cellular copy number
Periplasmic concentration (M)
22,000
20,000
18,000
16,000
14,000
12,000
10,000
8,000
6,000
4,000
2,000
0
1.2E-04
1.1E-04
1.0E-04
9.0E-05
8.0E-05
7.0E-05
6.0E-05
5.0E-05
4.0E-05
3.0E-05
2.0E-05
1.0E-05
0.0E+00
LivJ MetQ OppA LivK GlnH tcyj DppA HisJ GltI PotD ArtI ArgT ProX ArtJ GsiB PotF MppA YdcS SapA DdpA RbsB MglB MalE AraF XylF CysP ModA UgpB Sbp PstS ZnuA FepB thiB YnjB FecB BtuF FhuD
86.3
32.6
9
3.8
0.5
B
R² = 0.0133
MetQ
BtuF
FliY
DppA
Substrate binding affinity (Log K_A)
SBP periplasmic concentration (M)
C
R² = 0.9172
BtuF
ZnuA
MalE
FliY
ModA
HisJ
MetQ
TMD-SBP interaction affinity (Log K_A)
SBP periplasmic concentration (M)

Figure 2

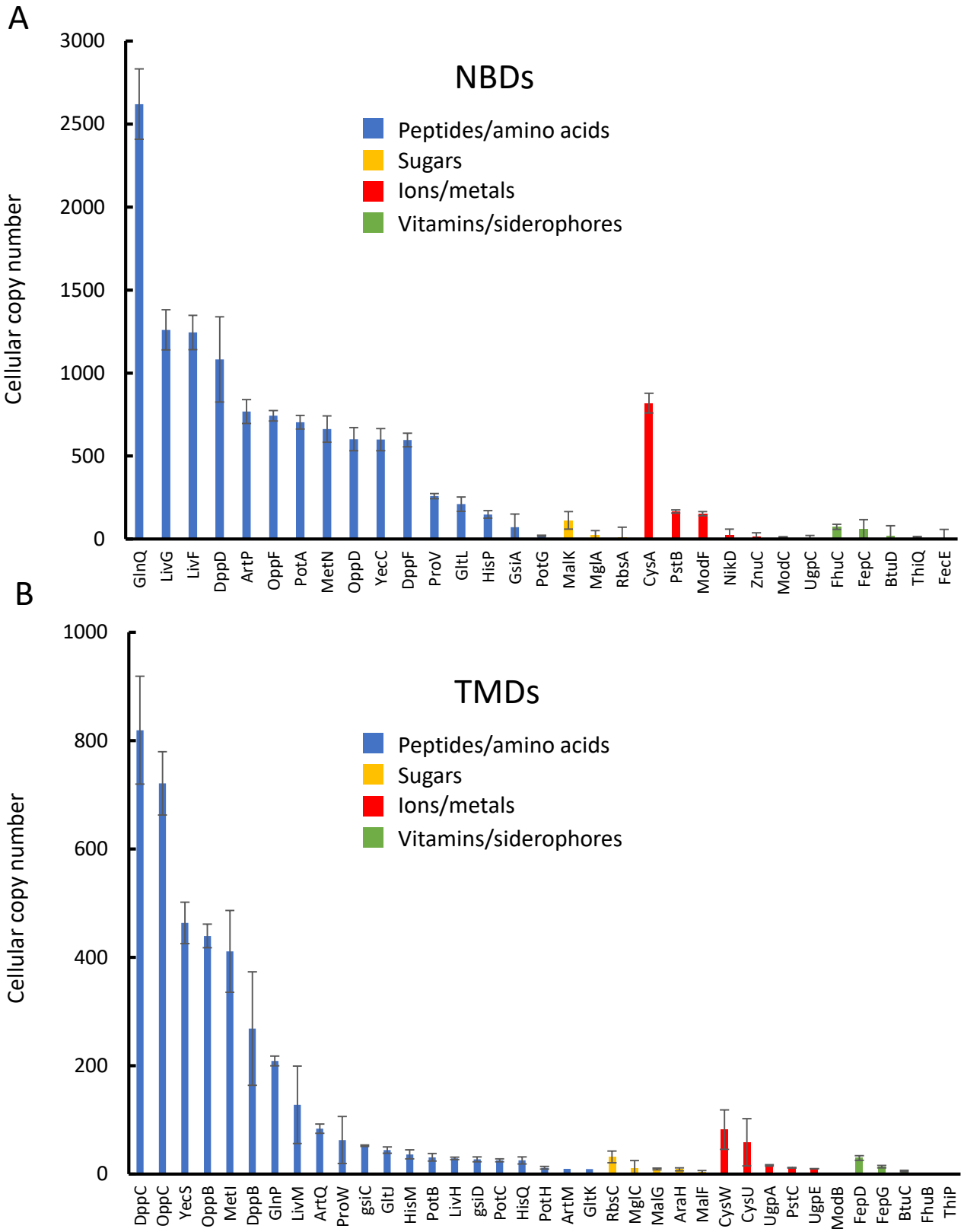
A
NBDs
Peptides/amino acids
Sugars
Ions/metals
Vitamins/siderophores
Cellular copy number
3000
2500
2000
1500
1000
500
0
GlnQ
LivG
LivF
DppD
ArtP
OppF
PotA
MetN
OppD
YecC
DppF
ProV
GltL
HisP
GsiA
PotG
MalK
MglA
RbsA
CysA
PstB
ModF
NikD
ZnuC
ModC
UgpC
FhuC
FepC
BtuD
ThiQ
FecE
B
TMDs
Peptides/amino acids
Sugars
Ions/metals
Vitamins/siderophores
Cellular copy number
1000
800
600
400
200
0
DppC
OppC
YecS
OppB
MetI
DppB
GlnP
LivM
ArtQ
ProW
gsiC
GltJ
HisM
PotB
LivH
gsiD
PotC
HisQ
PotH
ArtM
GltK
RbsC
MglC
MalG
AraH
MalF
CysW
CysU
UgpA
PstC
UgpE
ModB
FepD
FepG
BtuC
FhuB
ThiP

Figure 3

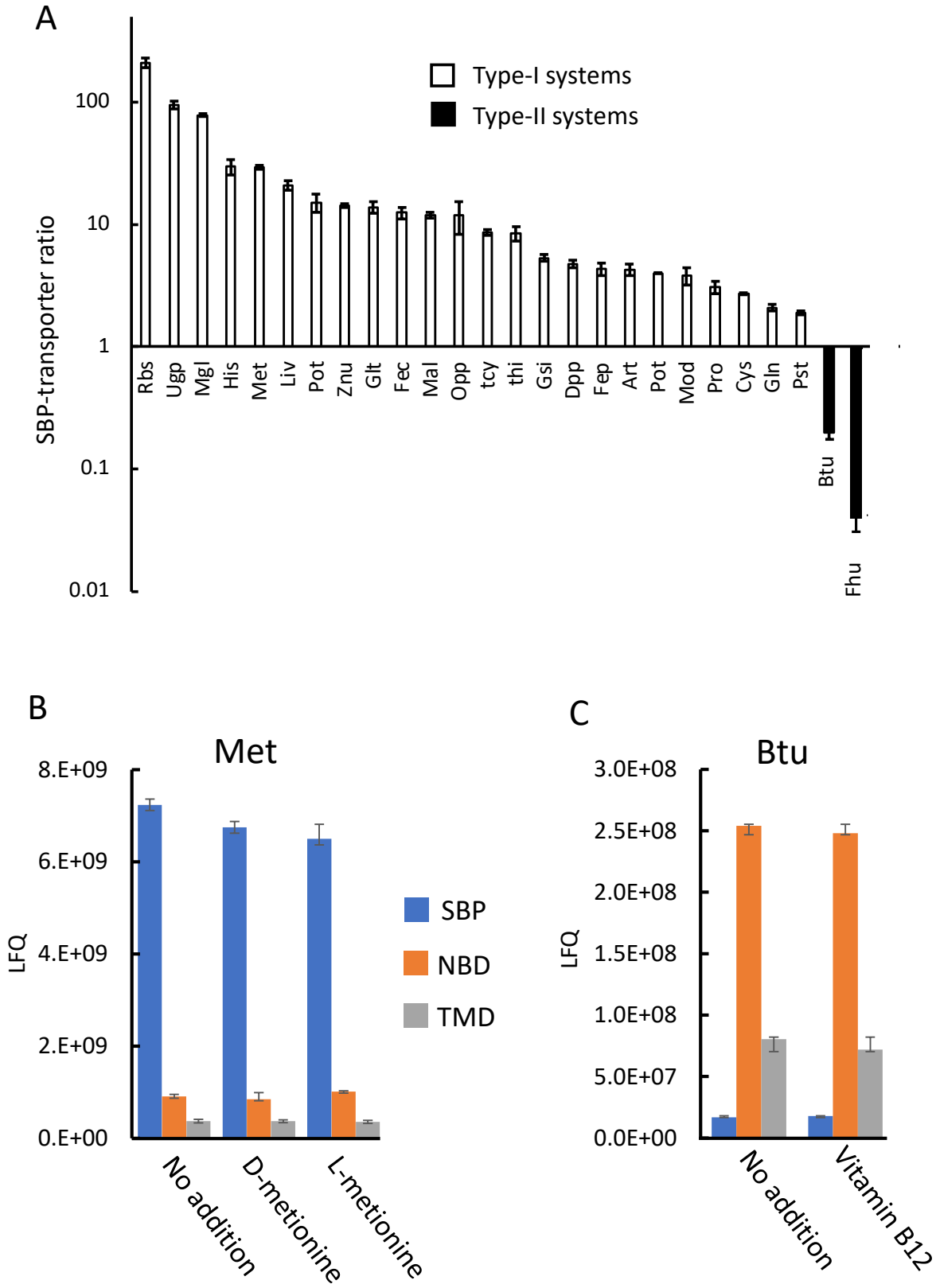
A
Type-I systems
Type-II systems
SBP-transporter ratio
100
10
1
0.1
0.01
Rbs
Ugp
Mgl
His
Met
Liv
Pot
Znu
Glt
Fec
Mal
Opp
tcy
thi
Gsi
Dpp
Fep
Art
Pot
Mod
Pro
Cys
Gln
Pst
Btu
Fhu
B
Met
LFQ
8.E+09
6.E+09
4.E+09
2.E+09
0.E+00
SBP
NBD
TMD
No addition
D-metionine
L-metionine
C
Btu
LFQ
3.0E+08
2.5E+08
2.0E+08
1.5E+08
1.0E+08
5.0E+07
0.0E+00
No addition
Vitamin B12

Figure 4

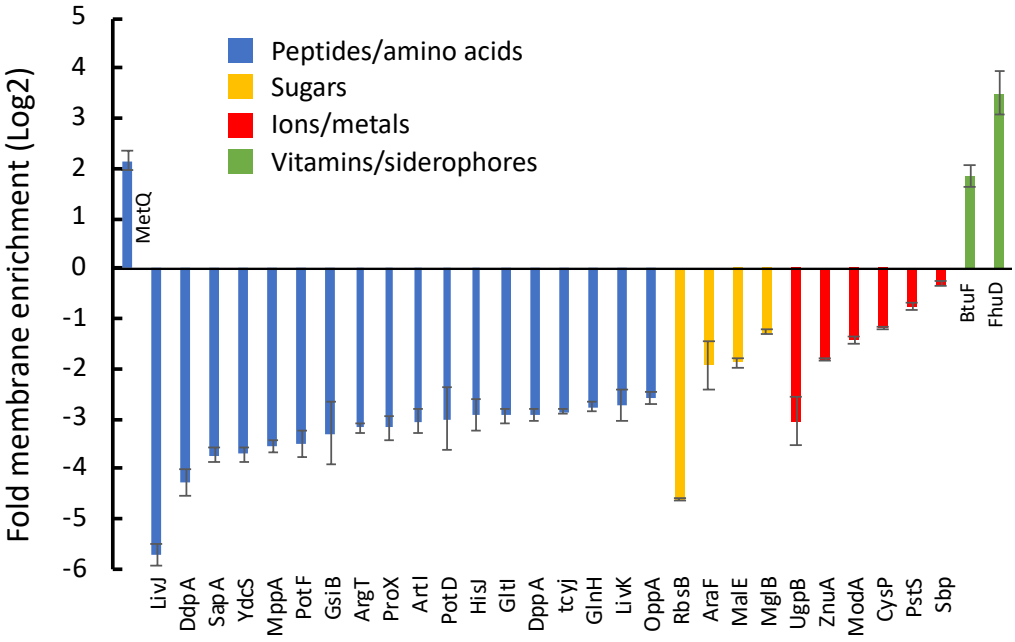
Fold membrane enrichment (Log2)
5
4
3
2
1
0
-1
-2
-3
-4
-5
-6
Peptides/amino acids
Sugars
Ions/metals
Vitamins/siderophores
MetQ
LivJ
DdpA
SapA
YdcS
MppA
PotF
GsiB
ArgT
ProX
ArtI
PotD
HisJ
GltI
DppA
tcyJ
GlnH
LivK
OppA
RbsB
AraF
MalE
MglB
UgpB
ZnuA
ModA
CysP
PstS
Sbp
BtuF
FhuD

Figure 5

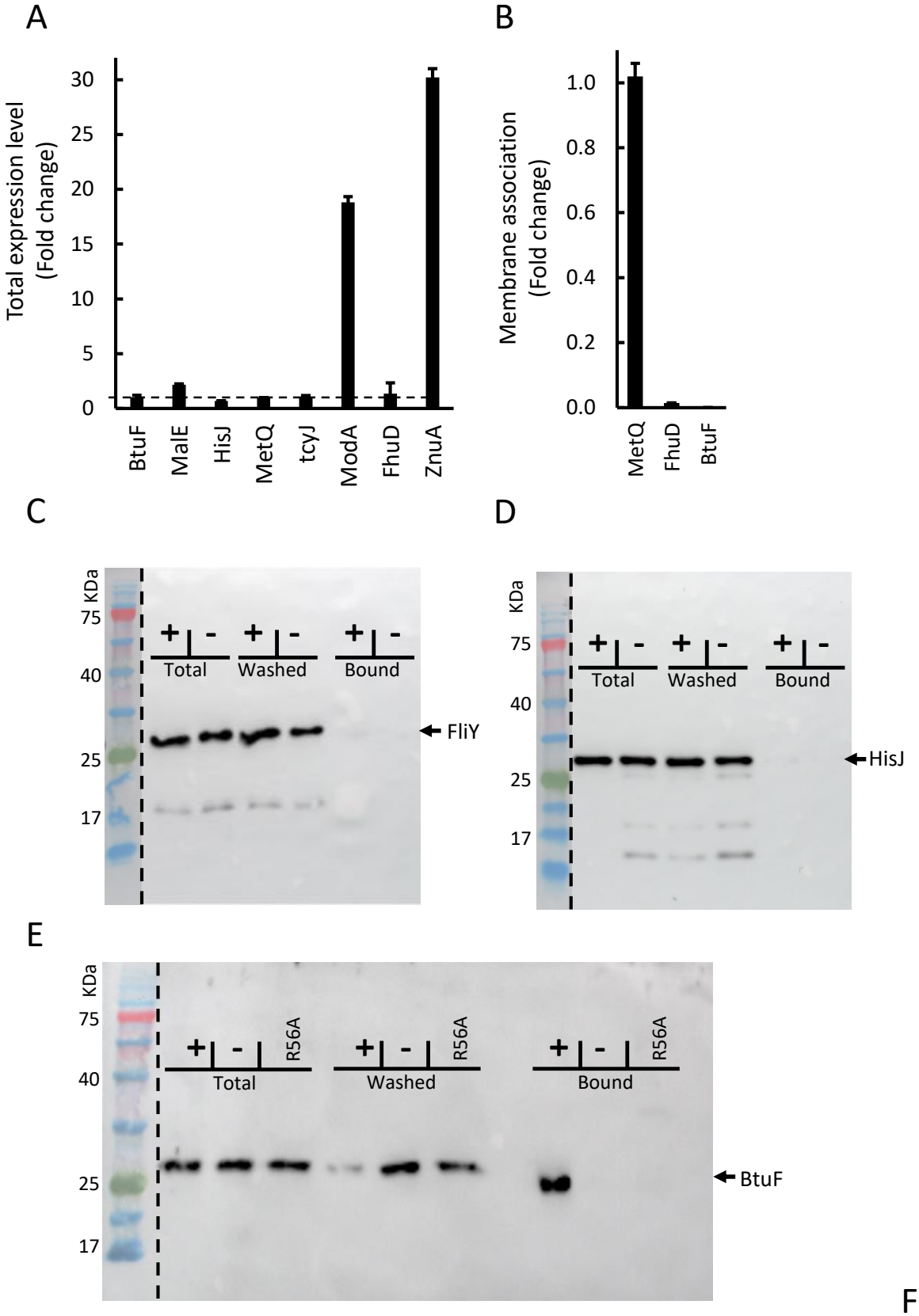
A
Total expression level
(Fold change)
30
25
20
15
10
5
0
BtuF
MalE
HisJ
MetQ
tcyJ
ModA
FhuD
ZnuA
B
Membrane association
(Fold change)
1.0
0.8
0.6
0.4
0.2
0.0
MetQ
FhuD
BtuF
C
KDa
75
40
25
17
+
-
Total
Washed
Bound
FliY
D
KDa
75
40
25
17
+
-
Total
Washed
Bound
HisJ
E
KDa
75
40
25
17
+
-
R56A
Total
Washed
Bound
BtuF

Figure 6

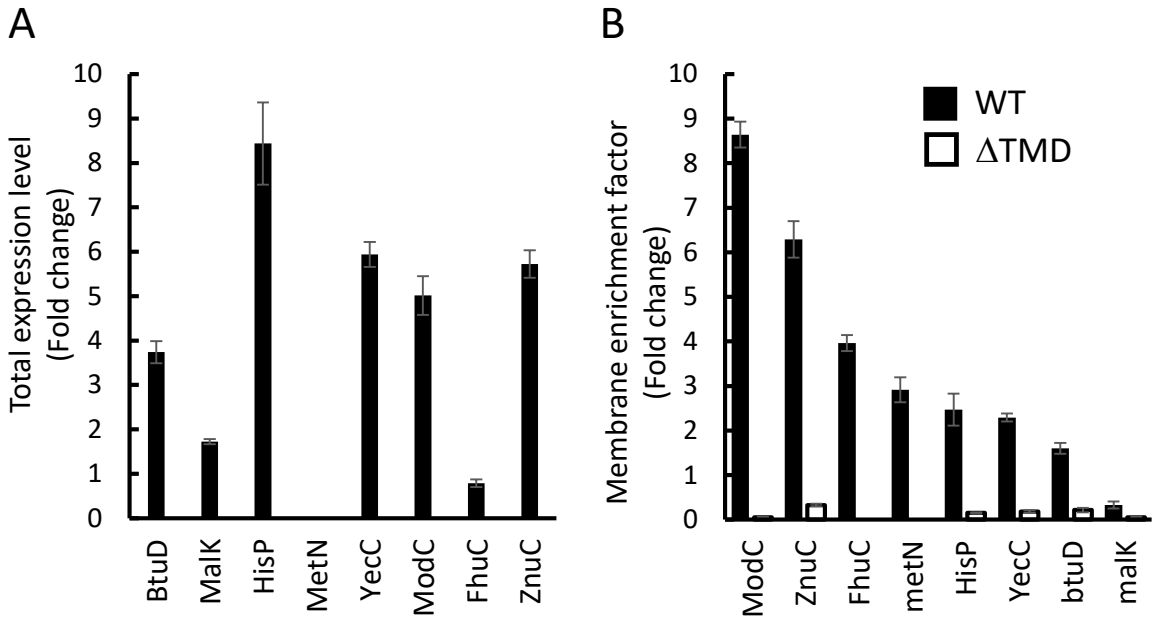
A
Total expression level
(Fold change)
10
9
8
7
6
5
4
3
2
1
0
BtuD
MalK
HisP
MetN
YecC
ModC
FhuC
ZnuC
B
Membrane enrichment factor
(Fold change)
WT
ΔTMD
ModC
ZnuC
FhuC
metN
HisP
YecC
btuD
malK

Figure 7

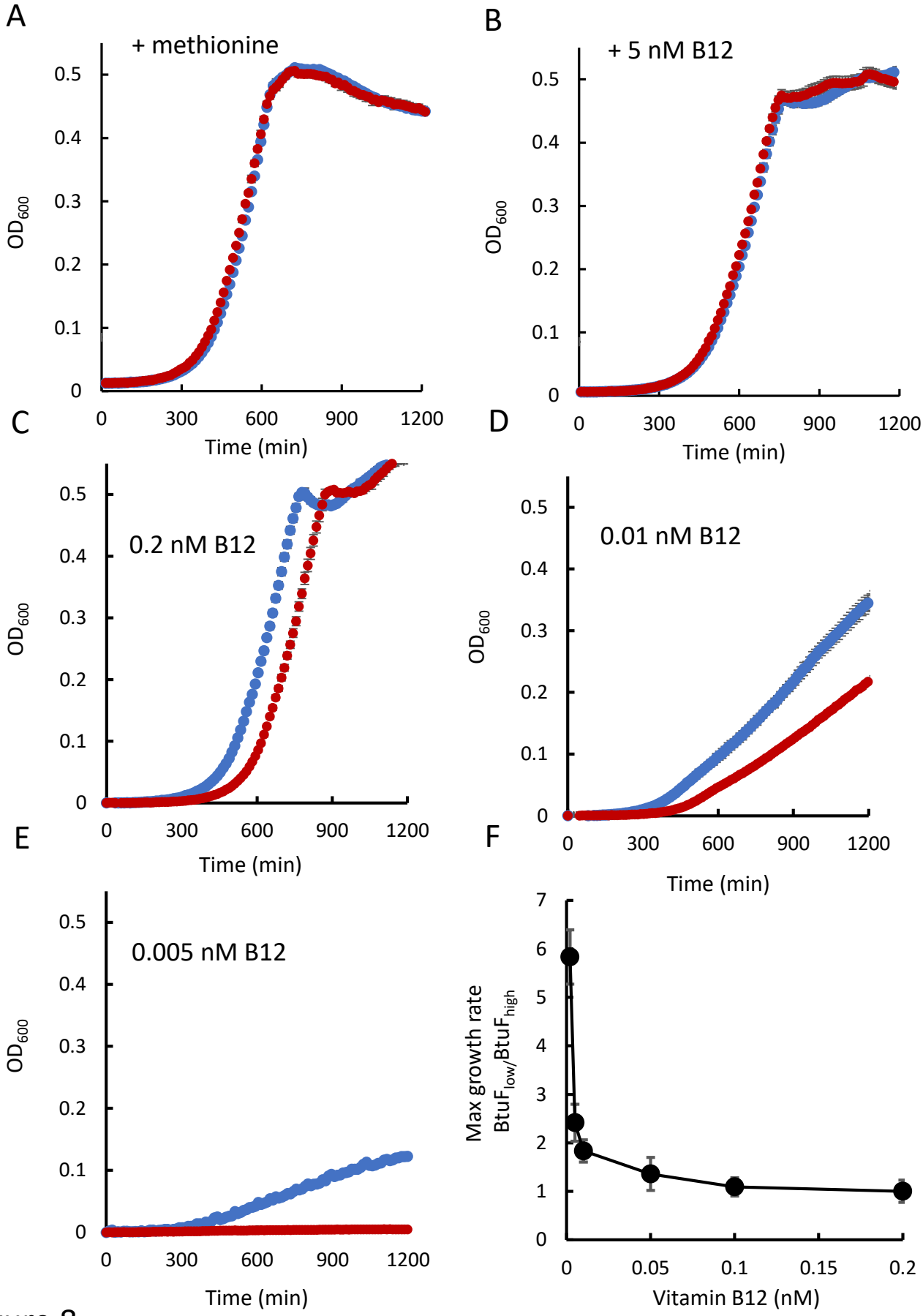
A
+ methionine
B
+ 5 nM B12
C
0.2 nM B12
D
0.01 nM B12
E
0.005 nM B12
F
OD600
Time (min)
0
0.1
0.2
0.3
0.4
0.5
300
600
900
1200
Max growth rate
BtuFlow/BtuFhigh
Vitamin B12 (nM)
0.05
0.15
1
2
3
4
5
6
7

Figure 8

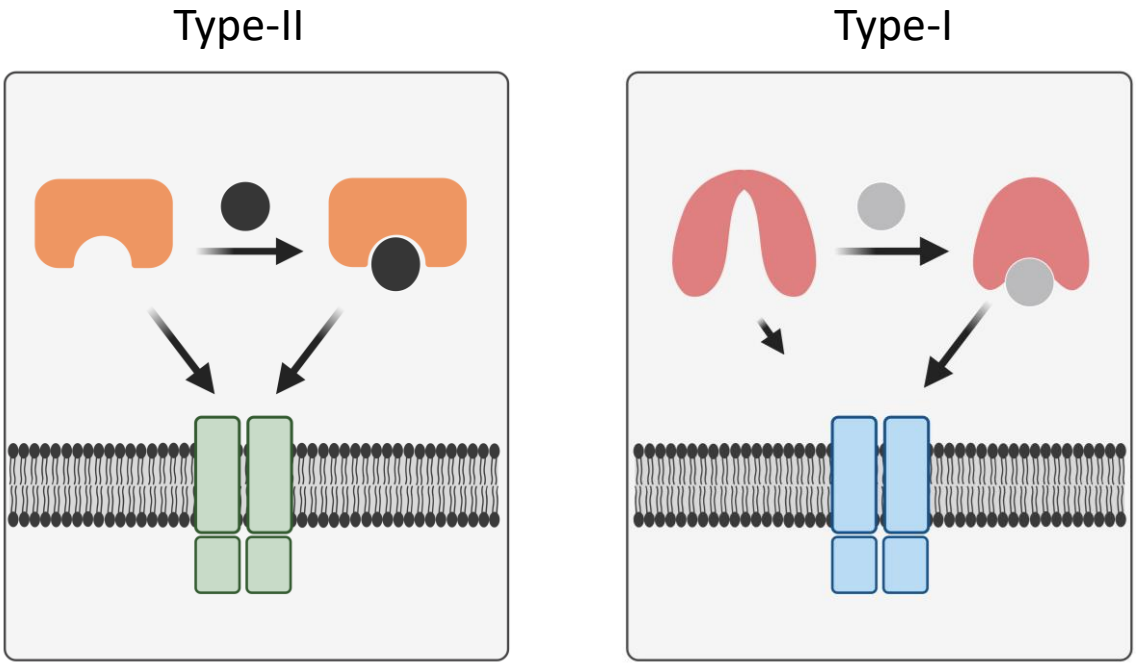

Figure 9

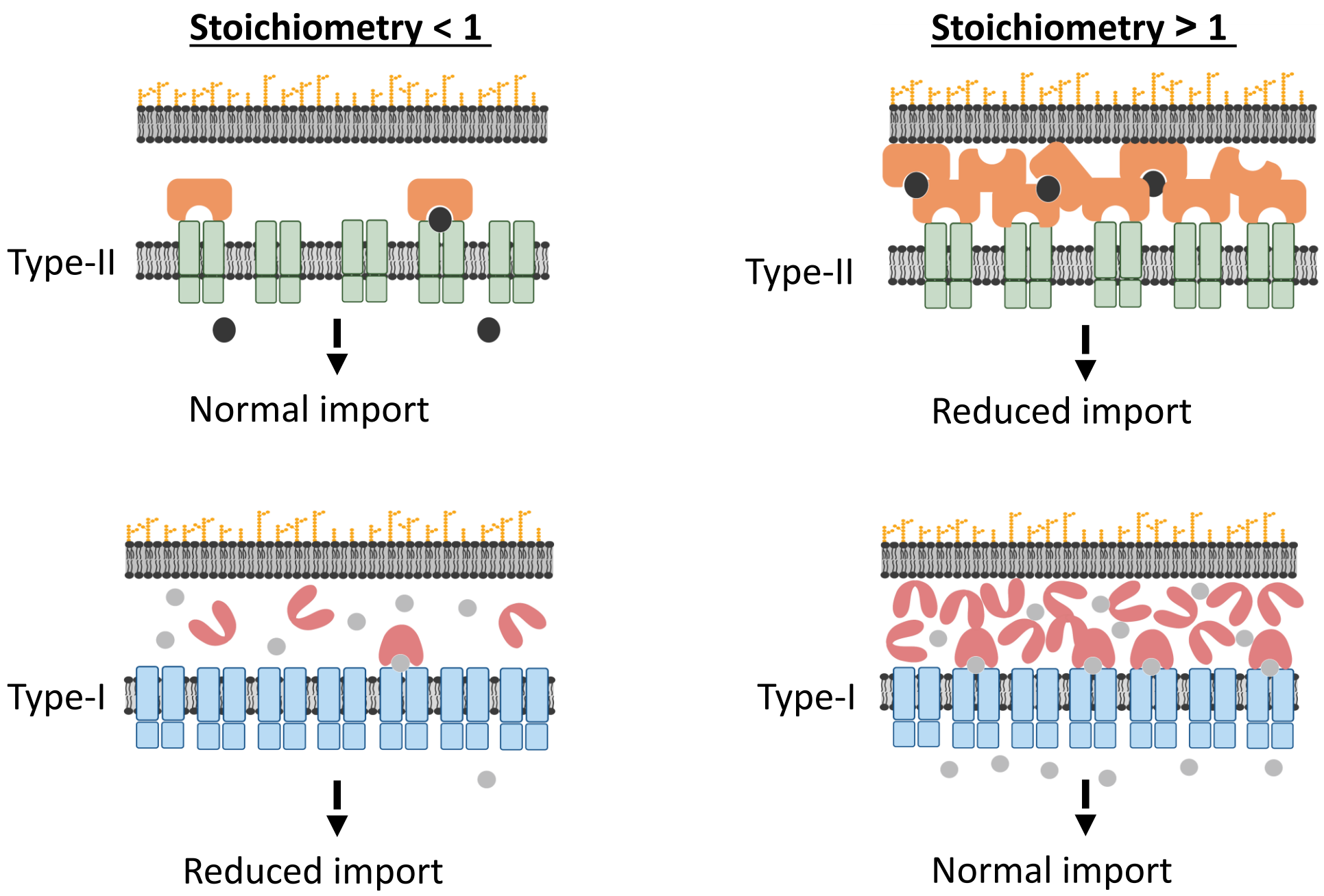
Stoichiometry < 1
Stoichiometry > 1
Type-II
Type-II
Normal import
Reduced import
Type-I
Type-I
Reduced import
Normal import

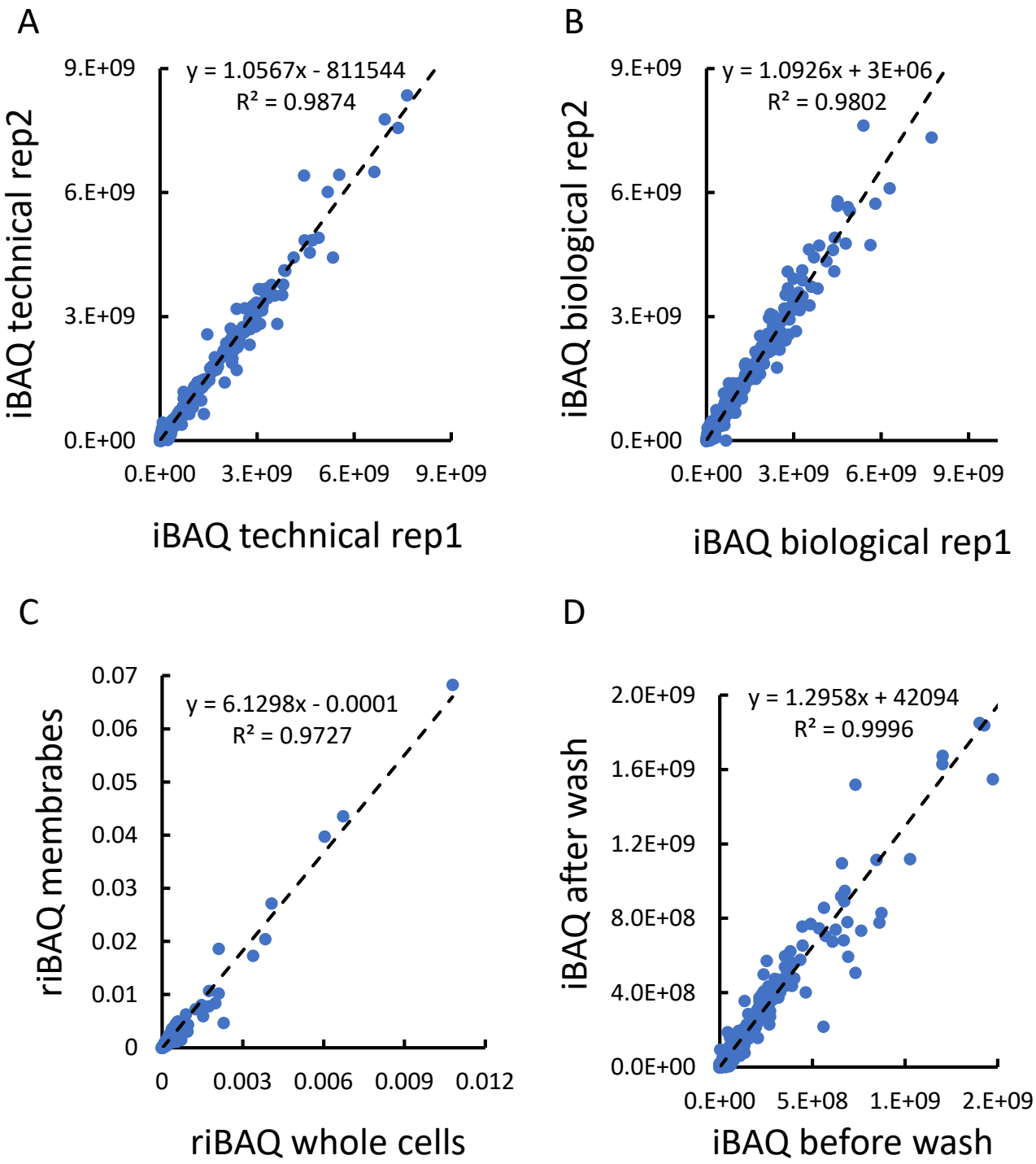
A
y = 1.0567x - 811544
R² = 0.9874
iBAQ technical rep2
iBAQ technical rep1
9.E+09
6.E+09
3.E+09
0.E+00
0.E+00
3.E+09
6.E+09
9.E+09
B
y = 1.0926x + 3E+06
R² = 0.9802
iBAQ biological rep2
iBAQ biological rep1
9.E+09
6.E+09
3.E+09
0.E+00
0.E+00
3.E+09
6.E+09
9.E+09
C
y = 6.1298x - 0.0001
R² = 0.9727
riBAQ membrabes
riBAQ whole cells
0.07
0.06
0.05
0.04
0.03
0.02
0.01
0
0
0.003
0.006
0.009
0.012
D
y = 1.2958x + 42094
R² = 0.9996
iBAQ after wash
iBAQ before wash
2.0E+09
1.6E+09
1.2E+09
8.0E+08
4.0E+08
0.0E+00
0.E+00
5.E+08
1.E+09
2.E+09

Figure S1

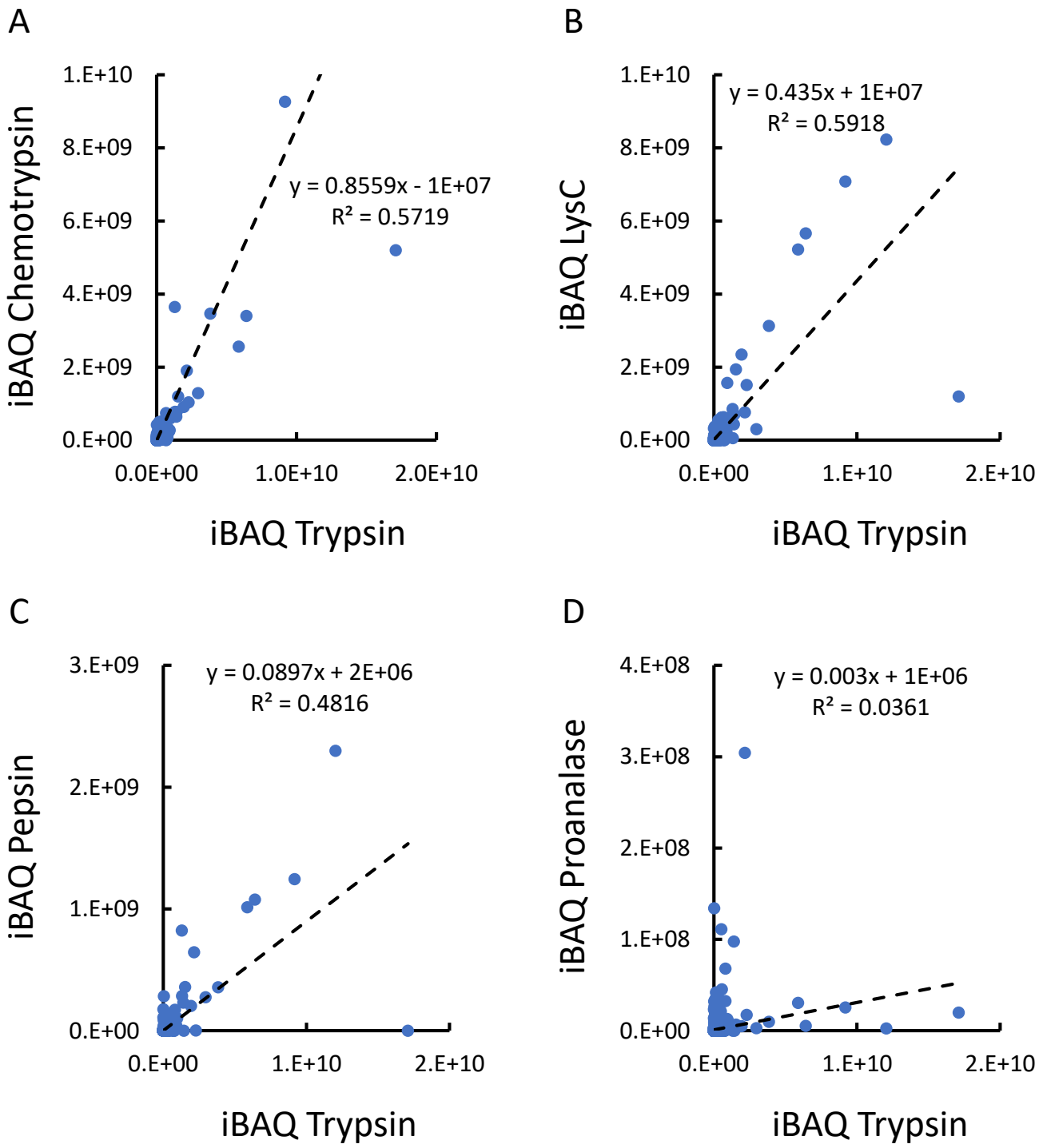
A
iBAQ Chemotrypsin
1.E+10
8.E+09
6.E+09
4.E+09
2.E+09
0.E+00
0.0E+00
1.0E+10
2.0E+10
iBAQ Trypsin
y = 0.8559x - 1E+07
R² = 0.5719
B
iBAQ LysC
1.E+10
8.E+09
6.E+09
4.E+09
2.E+09
0.E+00
0.E+00
1.E+10
2.E+10
iBAQ Trypsin
y = 0.435x + 1E+07
R² = 0.5918
C
iBAQ Pepsin
3.E+09
2.E+09
1.E+09
0.E+00
0.E+00
1.E+10
2.E+10
iBAQ Trypsin
y = 0.0897x + 2E+06
R² = 0.4816
D
iBAQ Proanalase
4.E+08
3.E+08
2.E+08
1.E+08
0.E+00
0.E+00
1.E+10
2.E+10
iBAQ Trypsin
y = 0.003x + 1E+06
R² = 0.0361

Figure S2

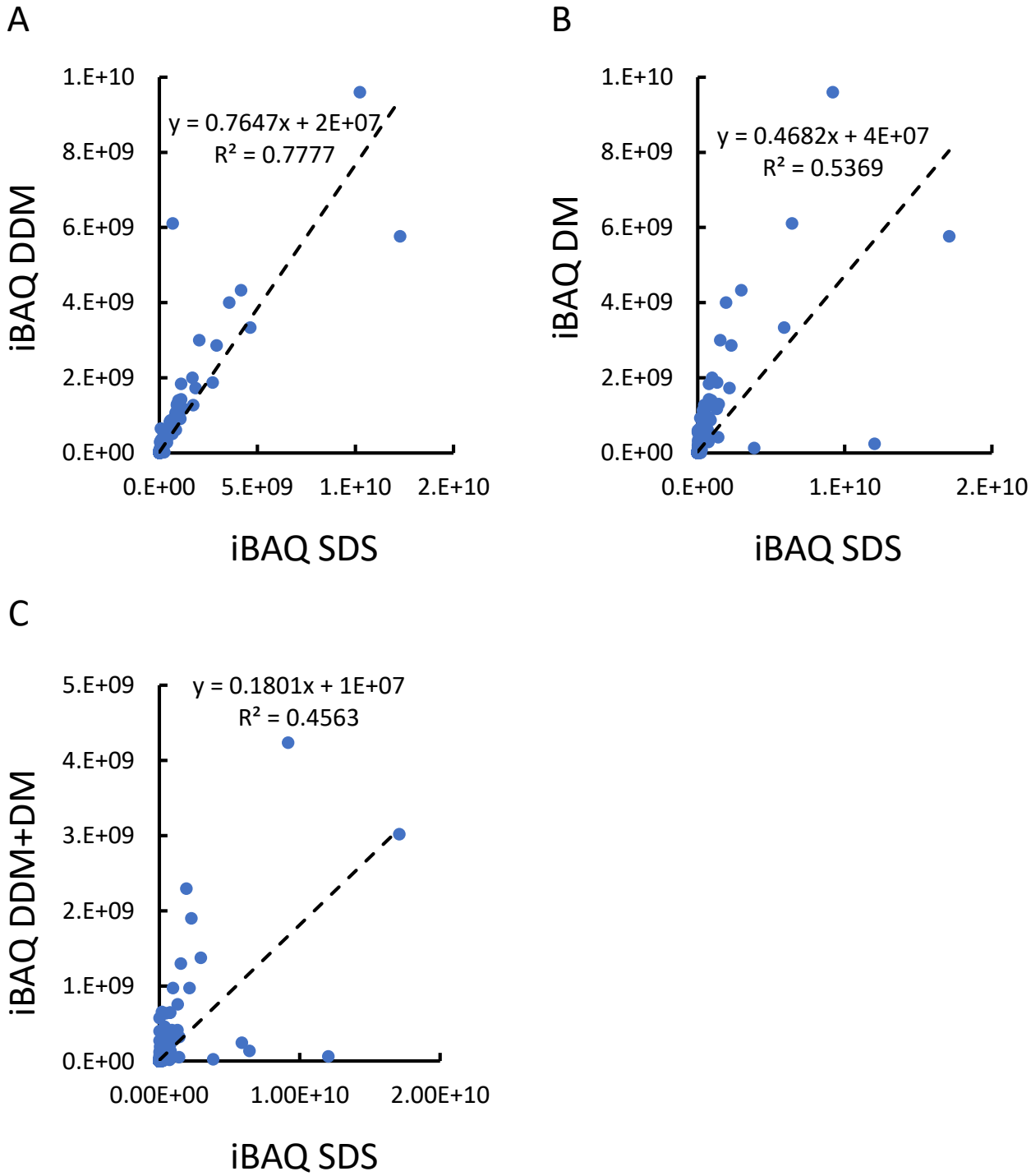
A
y = 0.7647x + 2E+07
R² = 0.7777
iBAQ DDM
iBAQ SDS
1.E+10
8.E+09
6.E+09
4.E+09
2.E+09
0.E+00
0.E+00
5.E+09
1.E+10
2.E+10
B
y = 0.4682x + 4E+07
R² = 0.5369
iBAQ DM
iBAQ SDS
1.E+10
8.E+09
6.E+09
4.E+09
2.E+09
0.E+00
0.E+00
1.E+10
2.E+10
C
y = 0.1801x + 1E+07
R² = 0.4563
iBAQ DDM+DM
iBAQ SDS
5.E+09
4.E+09
3.E+09
2.E+09
1.E+09
0.E+00
0.00E+00
1.00E+10
2.00E+10

Figure S3

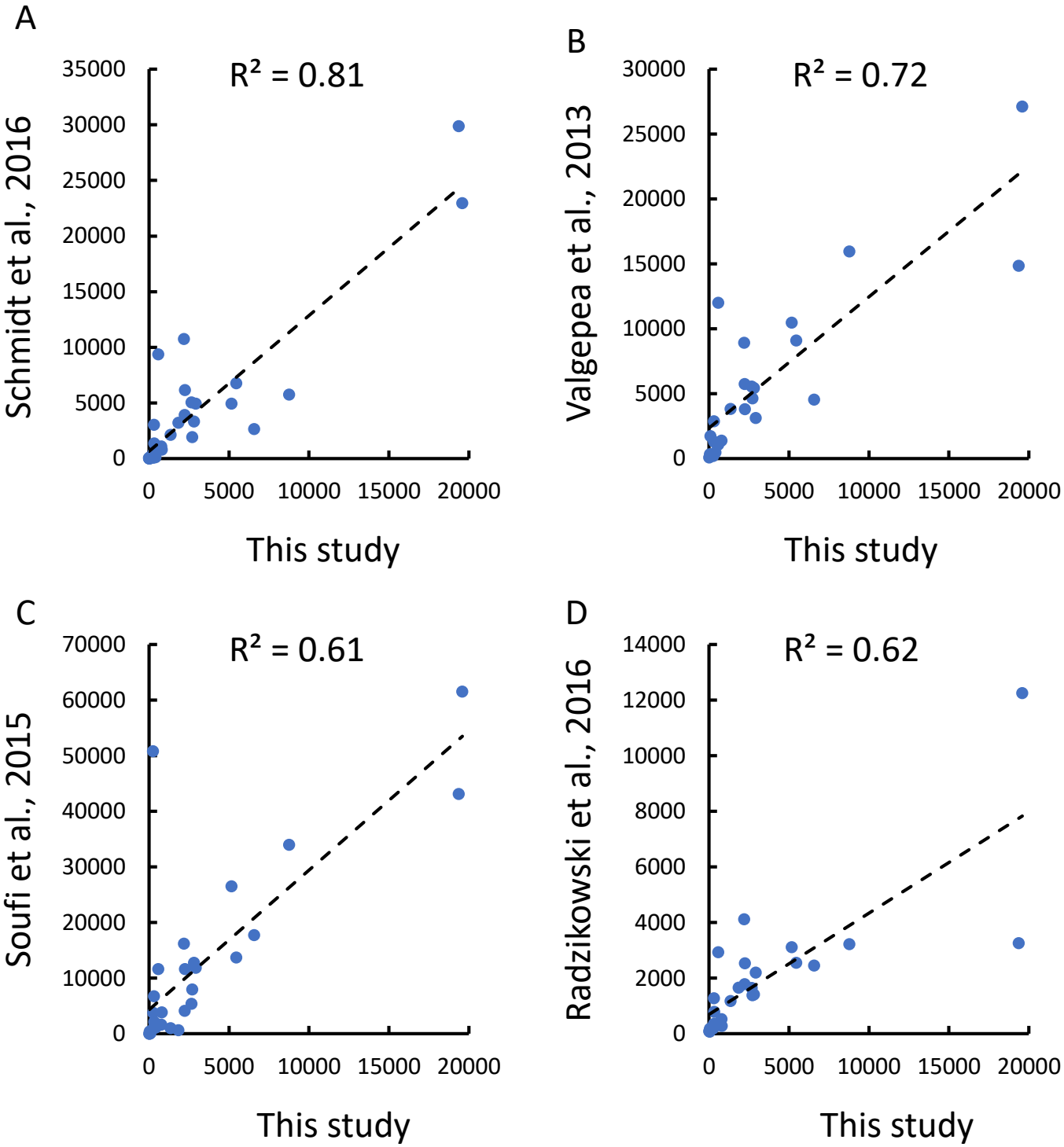
A
R² = 0.81
Schmidt et al., 2016
This study
B
R² = 0.72
Valgepea et al., 2013
This study
C
R² = 0.61
Soufi et al., 2015
This study
D
R² = 0.62
Radzikowski et al., 2016
This study

Figure S4

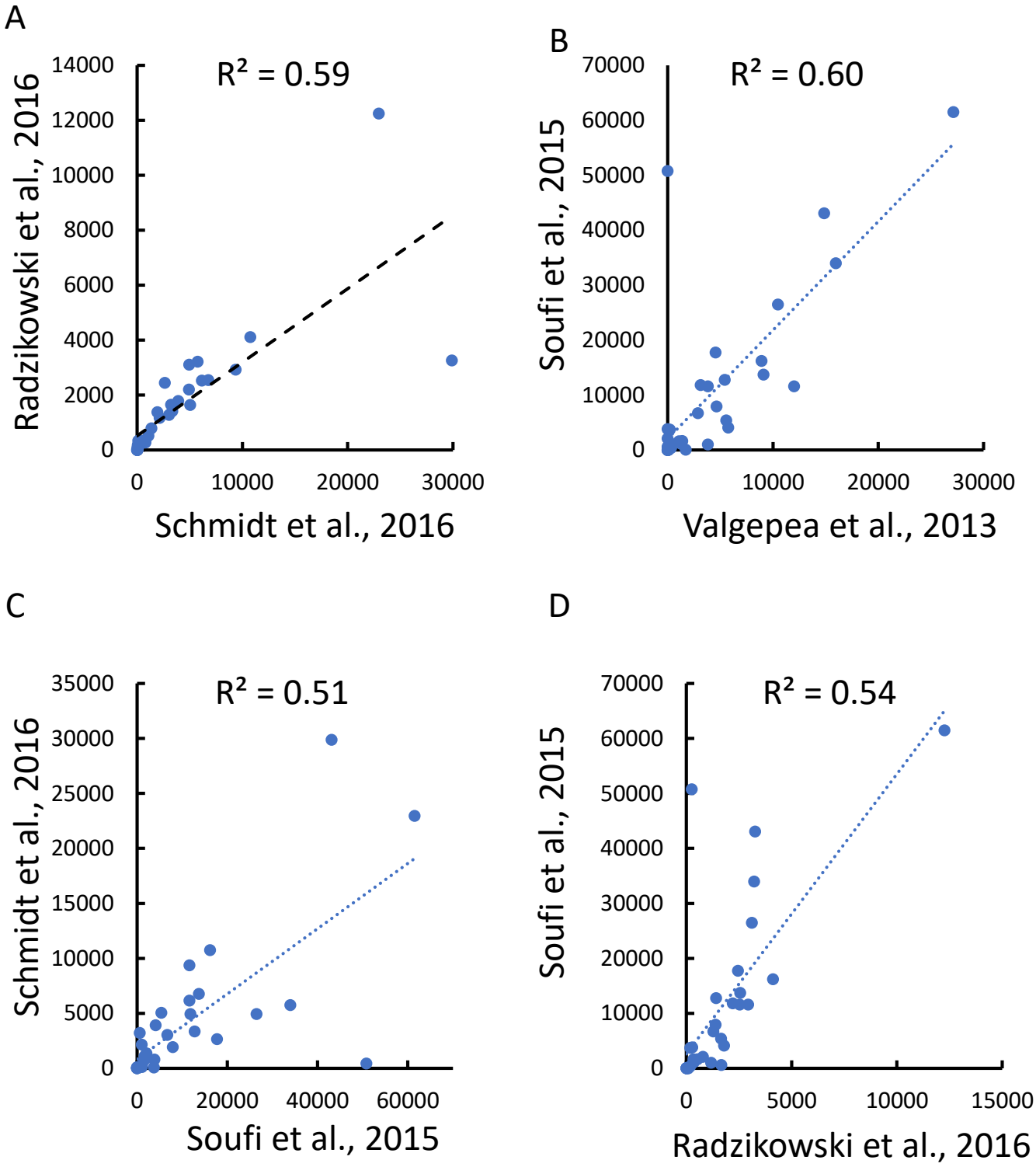
A
R² = 0.59
Radzikowski et al., 2016
Schmidt et al., 2016
0
2000
4000
6000
8000
10000
12000
14000
0
10000
20000
30000
B
R² = 0.60
Soufi et al., 2015
Valgepea et al., 2013
0
10000
20000
30000
40000
50000
60000
70000
0
10000
20000
30000
C
R² = 0.51
Schmidt et al., 2016
Soufi et al., 2015
0
5000
10000
15000
20000
25000
30000
35000
0
20000
40000
60000
D
R² = 0.54
Soufi et al., 2015
Radzikowski et al., 2016
0
10000
20000
30000
40000
50000
60000
70000
0
5000
10000
15000

Figure S5

A

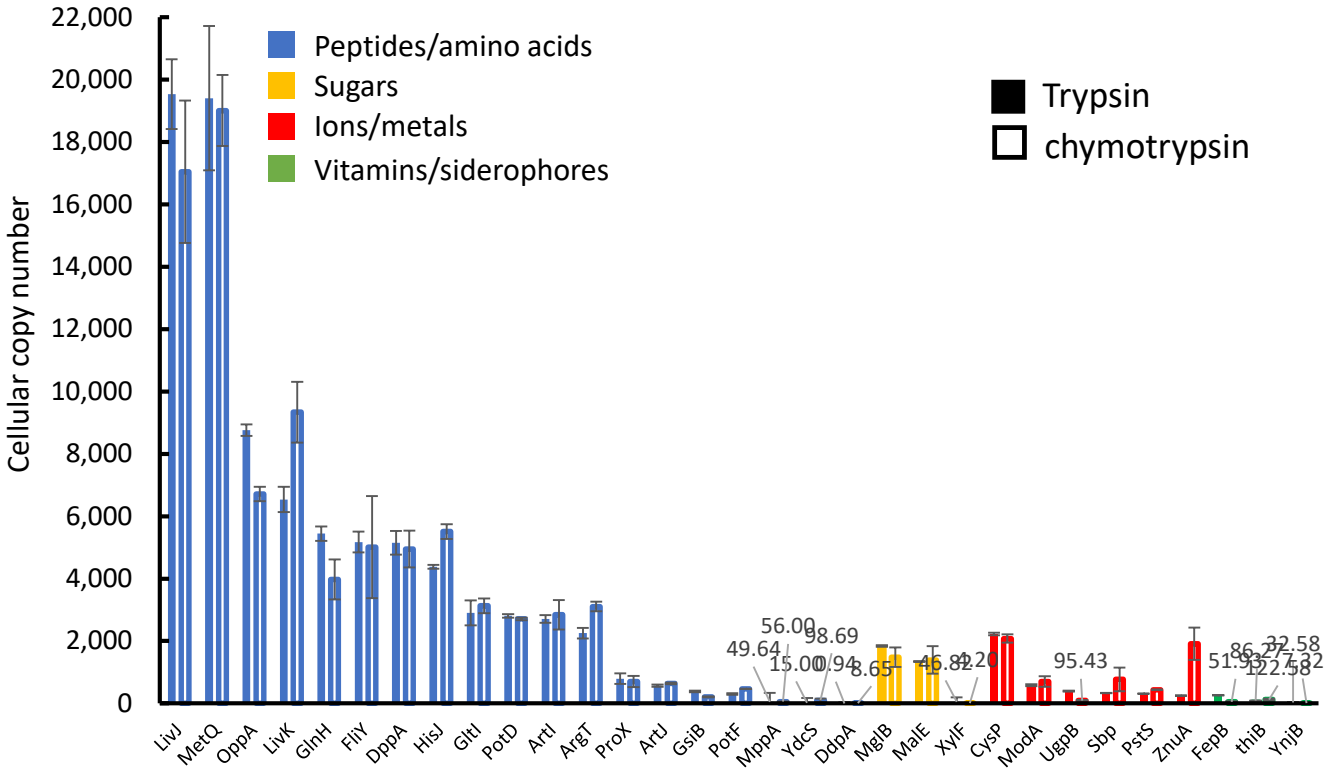
Cellular copy number
22,000
20,000
18,000
16,000
14,000
12,000
10,000
8,000
6,000
4,000
2,000
0
Peptides/amino acids
Sugars
Ions/metals
Vitamins/siderophores
Trypsin
chymotrypsin
LivJ
MetQ
OppA
LivK
GlnH
FliY
DppA
HisJ
GltI
PotD
ArtI
ArgT
ProX
ArtJ
GsiB
PotF
MppA
YdcS
DdpA
MglB
MalE
XylF
CysP
ModA
UgpB
Sbp
PstS
ZnuA
FepB
thiB
YnjB
56.00
49.64
98.69
95.43
32.58

B

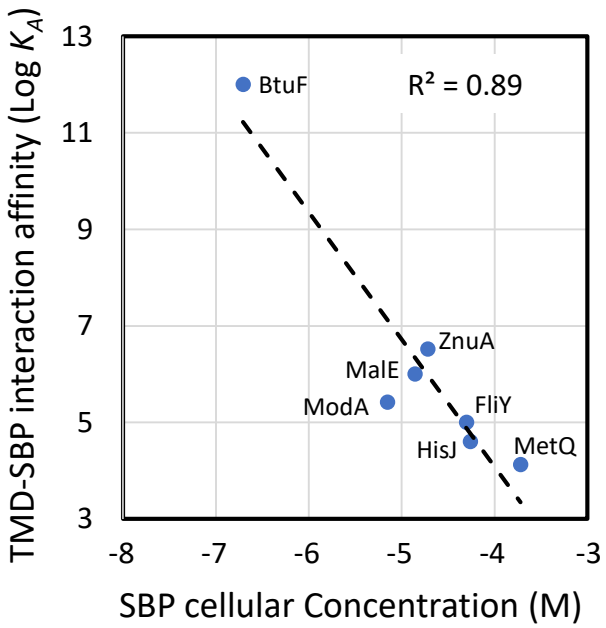
TMD-SBP interaction affinity (Log K_A)
13
11
9
7
5
3
BtuF
R^2 = 0.89
ZnuA
MalE
ModA
FliY
HisJ
MetQ
-8
-7
-6
-5
-4
-3
SBP cellular Concentration (M)

Figure S6

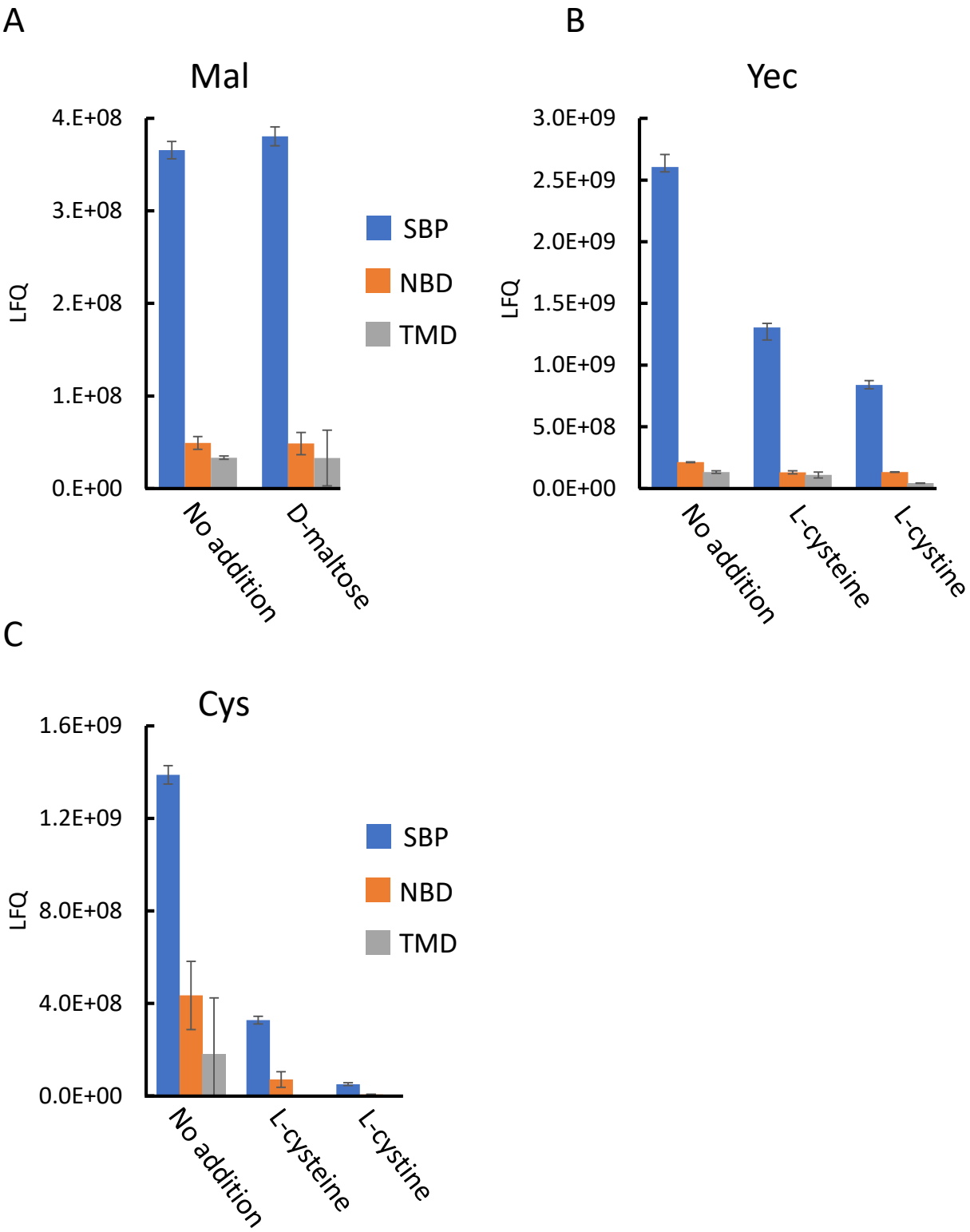
A
Mal
4.E+08
3.E+08
2.E+08
1.E+08
0.E+00
LFQ
SBP
NBD
TMD
No addition
D-maltose
B
Yec
3.0E+09
2.5E+09
2.0E+09
1.5E+09
1.0E+09
5.0E+08
0.0E+00
LFQ
No addition
L-cysteine
L-cystine
C
Cys
1.6E+09
1.2E+09
8.0E+08
4.0E+08
0.0E+00
LFQ
SBP
NBD
TMD
No addition
L-cysteine
L-cystine

Figure S7

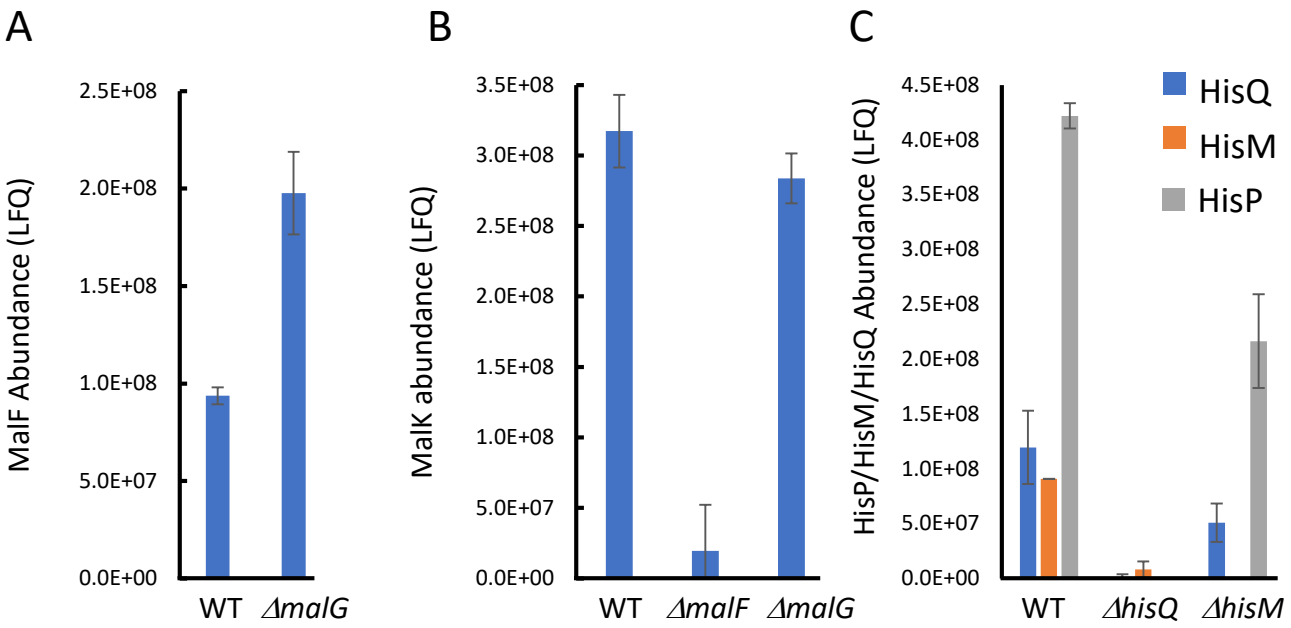
A
MalF Abundance (LFQ)
2.5E+08
2.0E+08
1.5E+08
1.0E+08
5.0E+07
0.0E+00
WT
ΔmalG
B
MalK abundance (LFQ)
3.5E+08
3.0E+08
2.5E+08
2.0E+08
1.5E+08
1.0E+08
5.0E+07
0.0E+00
WT
ΔmalF
ΔmalG
C
HisP/HisM/HisQ Abundance (LFQ)
4.5E+08
4.0E+08
3.5E+08
3.0E+08
2.5E+08
2.0E+08
1.5E+08
1.0E+08
5.0E+07
0.0E+00
HisQ
HisM
HisP
WT
ΔhisQ
ΔhisM

Figure S8